EXTREME SILICON ISOTOPE FRACTIONATION DUE TO Si ORGANIC COMPLEXATION: IMPLICATIONS FOR SILICA BIOMINERALIZATION

Franziska M. Stamm[a*], Merlin Méheut[a], Thomas Zambardi[b], Jérôme Chmeleff[a], Jacques Schott[a], Eric H. Oelkers[a,c*]

Affiliations:

a Géosciences Environnement Toulouse, CNRS-UPS-OMP, 14 av. Édouard Belin, 31400 Toulouse, France

b LEGOS, Laboratoire d'Etudes en Géophysique et Océanographie Spatiales (CNRS/UPS/CNES/IRD), Observatoire Midi-Pyrénées14 Avenue Edouard Belin, 31400 Toulouse, France

c Department of Earth Sciences, UCL, Gower Street, WC1E 6BT London, United Kingdom

***Corresponding authors:**

Franziska M. Stamm: Current address: Department of Geology Lund University, Sölvegatan 12, 223 62 Lund, Sweden; **e-mail:** stamm.fm@gmail.com

Eric H.Oelkers: Department of Earth Sciences, UCL, Gower Street, WC1E 6BT London, United Kingdom; **e-mail:** e.oelkers@ucl.ac.uk

Abstract

A combination of theoretical predictions and isotopic equilibration experiments using the three-isotope method have been performed to assess Si isotope fractionation among minerals, and aqueous species in the presence of dissolved catechol. Aqueous Si in abiotic ambient temperature aqueous solutions is dominated by the IV-coordinated $H_4SiO_4^0$ species, but the presence of aqueous catechol provokes the formation of a VI-fold Si-catechol complex. Results show an equilibrium Si fractionation factor of ~ 19‰ between the VI-fold coordinated Si-catechol complex and the IV-fold coordinated aqueous silicic acid, an amplitude never previously observed for silicon. The fractionation between V-fold Si-organo complexes (with diolate, glyconate or methyllactate groups) and silicic acid has also been estimated through theoretical predictions to be about -10‰. These extreme fractionations can be used to improve our ability to interpret the Si isotope compositions of natural solids, and in particular those associated with marine silica biomineralization processes (e.g. sponge spicules).

Keywords: Silicon; equilibrium isotope fractionation; organo-silicon complexes; first principle calculation; three-isotope method; Si coordination change

1. Introduction

Silicon (Si) enters the biogeochemical cycle through the weathering of silicate minerals, and circulates through the biosphere as dissolved aqueous Si primarily as silicic acid ($H_4SiO_4^0$). Silicon occurs in numerous plants mostly as phytoliths, which enhance their structural stability and defensive mechanisms (e.g. Kubicki and Heaney, 2003; Poitrasson, 2017 and references therein). In higher organisms, such as animals or humans, it is used for bone or tissue formation (e.g. Jugdaohsingh et al., 2015). In marine environments Si is used by phytoplankton, zooplankton and sponges to form opaline structures, such as frustules, tests or spicules (Kubicki and Heaney, 2003; Hendry and Robinson, 2012; Poitrasson, 2017; Cassarino et al., 2018). Such 'bio-Si' has distinct isotopic signatures with $\delta^{30}Si$ values ranging from +3 to -6.5 ‰ (Poitrasson, 2017). In general, biogenic solids preferentially uptake light Si isotopes (e.g. Opfergelt et al., 2006; Hendry and Robinson, 2012; Cassarino et al., 2018). The lightest Si isotope composition reported so far in natural solids, between -5 -7 ‰, has been observed in sponges (Cassarino et al., 2018) and choanoflagellates (Marron et al., 2019). The processes and mechanisms generating these light Si isotope compositions are not yet fully understood (Kubicki and Heaney, 2003; Kinrade et al., 2002; Poitrasson, 2017; Cassarino et al., 2018). One possibility, however, is that the interaction between aqueous Si and organic matter could impact Si isotope fractionation (Kinrade et al., 2002; Cassarino et al., 2018).

Silicon can form aqueous complexes with a number of organic ligands including polyols, saccharides, phenols, pyridine and tropolones (Cella et al., 1980; Sjöberg et al., 1985; Kinrade et al., 2001a; Benner et al., 2003; Kubicki and Heaney, 2003). The formation of such complexes can alter the aqueous Si coordination environment. Past Nuclear Magnetic Resonance (NMR) studies have shown that Si, which usually occurs in natural waters as the IV-coordinated silicic acid ($H_4SiO_4^0$) complex can form V- and VI-coordinated organosilicon complexes in the presence of aqueous organic ligands such as phenols and

polyols (Cella et al., 1980; Kinrade et al., 2001a). Evidence of natural occurring VI-coordinated organosilicon compounds formed *in-vivo* has been provided by the ^{29}Si nuclear resonance study of the fresh water diatom *Navicula pelliculosa* (Kinrade et al., 2002). In general, coordination changes have been identified as a primary factor influencing isotopic fractionation (Schauble, 2004). Such is the case for example of boron, with an isotope fractionation of about -27 ‰ between boric acid ($H_3BO_3^0$ with trigonal B) and the borate ion (BO_4^-, tetragonal B; e.g. Balan et al., 2018)

This study investigates the effect of the change in Si coordination by aqueous organic Si complex formation on equilibrium Si isotope fractionation in water-rock systems. Catechol ($C_6H_4(OH)_2$) is used as a representative aqueous organic ligand, as it readily binds to Si (Barnum, 1970; Pokrovski and Schott, 1998) and changes the common IV-coordinated aqueous Si to a hexacoordinated complex with a 6-membered ring structure as shown in Fig. 1 (Sjöberg et al., 1985; Kinrade et al., 1999). To determine Si isotope equilibrium fractionation between silicic acid and the Si-catecholate complex, this study combines first-principle calculations and experiments performed using the three-isotope method performed at 25 °C and pH ~8.8 at equilibrium between amorphous silica and 0.05 M and 0.08 M catechol solutions. The results of this study provide new insight into the effects of aqueous organic complexation on Si isotope equilibrium fractionation in the bio- and hydrosphere.

2. Materials and Methods

2.1. Theoretical modelling

To assess the role of changing Si coordination due to aqueous organic complexation on its isotope fractionation properties, both VI-fold and V-fold coordination compounds were considered. These calculations were based on compounds modelled from X-ray determined structures found in the literature. As an example of VI-fold coordinated Si, $Li_2[Si(Cat)_3]$•3.5dme was considered (where cat = the catecholate dianion, and dme = dimethoxy ethane CH_3-O-CH_2-CH_2-O-CH_3; Hahn et al., 1995). For V-fold coordinated Si, three structures were considered, chosen for their different functional groups and coordination polyhedrons: $Li[Si(AnErytH_{-2})_2(OH)]\cdot H_2O$ (where $AnErytH_{-2}$=anhydroerythritol dianions; Benner et al., 1999), [2-(Dimethylammonio)ethoxy]bis[2-methyllactato(2-)-O^1,O^2] silicate (compound 7 of Tacke et al., 1999), and $Li[Si(OCH_2CH_2OH)\ (OCH_2CH_2O)_2]$ (compound 1 of Donhärl et al., 1998). These structures are assumed to be representative of VI- and V-fold coordinated aqueous Si and will be referred to as $SiCat_3^{2-}$, SiDio, SiLact and SiGly, respectively.

2.1.1. First-principle calculations of equilibrium Si isotope fractionation factors

The equilibrium fractionation of silicon isotopes between two phases is obtained by combining the β-factors of both phases. The β-factor corresponds to the isotopic fractionation factor between Si atoms in a phase compared to it as an ideal gas. This quantity can be computed within the harmonic approximation from the vibrational frequencies of the phase of interest (Bigeleisen and Mayer, 1947). Details of the calculation of the β-factor of quartz and of dissolved $H_4SiO_4^0$ with the harmonic approximation are given in Méheut et al. (2007) and Dupuis et al. (2015), respectively. The β-factors of hypervalent Si model structures in the present study were computed from their phonon frequencies at the Γ-point according to equation (5) of Dupuis et al. (2015). The phonon frequencies were computed

109 from first-principles using density functional theory (DFT; Hohenberg and Kohn, 1964;
110 Kohn and Sham, 1965). The calculation was based on two exchange-correlation functionals:
111 that of Perdew, Burke and Ernzerhof (PBE; Perdew et al., 1996), and the vdW-DF2 non-
112 local functional (Lee et al., 2010). It used a plane-wave basis set, and atomic
113 pseudopotentials as implemented in the Quantum Espresso package (Giannozzi et al., 2009).
114 The pseudopotentials used for Si, O and H are described in the electronic annexes of Méheut
115 et al. (2007). The pseudopotential used for Li was taken from the PSlibrary (Dal Corso,
116 2014). The pseudopotential used for C was taken from Füger et al. (2018). Electronic wave-
117 functions were expanded in plane-waves up to an energy cutoff ε_{cut} = 80 Ry and the charge
118 density cut-off is set to 4 ε_{cut}. The electronic structure calculation was performed at the Γ-
119 point of the first Brillouin zone for Si-catecholate ($SiCat_3^{2-}$), and at the Baldereschi point
120 (Baldereschi, 1973) for Si-diolate (SiDio), Si-lactate (SiLact) and Si-glyconate (SiGly).
121 Phonon frequencies were computed using linear response theory (Baroni et al., 2001) and
122 the Quantum Espresso package (Giannozzi et al., 2009). The calculated structural properties
123 (Table A.1), vibrational properties (Fig. A.2) and the derived fractionation properties (Figs.
124 A.1, A.3, A.4) are discussed in detail in the Supplemental Information A.
125
126 **2.1.2. Speciation calculations**
127 Speciation calculations for all aqueous solutions used in this study were performed
128 using the PHREEQC code (Parkhurst and Appelo, 2013) together with its llnl
129 thermodynamic database. The equilibrium constant for the amorphous SiO_2 dissolution
130 reaction of the llnl database was changed to match that reported by Stamm et al. (2019); this
131 value was obtained on the same amorphous SiO_2 powder as used in the present study.
132 Furthermore the dissociation constants of aqueous catechol from Sillen and Martell (1971)
133 and the formation constant of the Si-catechol complex from Pokrovski and Schott (1998)
134 summarized in the Supplemental Table B.1 were added to the llnl database.

The equilibrium fractionation factor between the aqueous solution and amorphous silica depends on the Si speciation of the solution, and the individual fractionation factors, $\alpha_{i-SiO_2,am}^{x/28}$, of each of the *i*th Si aqueous species with respect to amorphous silica. The Si isotopic fractionation factor between the solution and amorphous silica is the weighted sum of the fractionation factors of each species such that (Zhang et al., 1995):

$$10^3 ln\alpha_{fluid-SiO_2,am}^{x/28} = \sum_i (x_i \times 10^3 ln\alpha_{i-SiO_2,am}^{x/28}) \quad (1)$$

where x_i refers to the mole fraction of the subscripted Si aqueous species present in the fluid. Note that Si isotopic fractionation between the fluid and SiO_2,am, $\Delta^x Si_{fluid\text{-}SiO_2,am}$ is approximately related to $\alpha_{fluid-SiO_2,am}^{x/28}$ by

$$\Delta^x Si_{fluid\text{-}SiO_2,am} \approx 10^3 ln\alpha_{fluid-SiO_2,am}^{x/28} \quad (2)$$

2.2. Experimental approach

2.2.1. Experimental design.

The three-isotope method was used to determine the equilibrium isotopic fractionation factor between aqueous catechol solutions and SiO_2,am. This method permits the determination of the degree of isotopic exchange (*F*) between the solid and its coexisting aqueous solution after adding a ^{29}Si tracer to the aqueous phase. A detailed description of this method is given in previous studies (e.g. Matsuhisa et al., 1978; Stamm et al., 2019). In brief the equilibrium isotopic composition of amorphous silica ($\delta^{30}Si_{SiO_2,am}$) and the fluid ($\delta^{30}Si_{fluid}$) were obtained from the linear extrapolation of $\delta^{30}Si$ values to 100% isotope exchange. This extrapolation was facilitated by plotting of measured $\delta^{30}Si_{fluid}$ and $\delta^{30}Si_{SiO_2,am}$ as a function of the degree of isotopic exchange *F*. *F* was calculated using

$$F = \frac{(\delta_t - \delta_i)}{(\delta_e - \delta_i)} \quad (3)$$

where δ_t denotes δ^{29}Si of the fluid at any time t during the reaction, and δ_i and δ_e describe the initial and equilibrium δ^{29}Si value of the fluid, respectively; δ_e was deduced iteratively from mass balance considerations. A detailed description of these mass balance calculations is given by Stamm et al. (2019).

All isotope equilibration experiments performed in this study were conducted at bulk chemical equilibrium but isotopic disequilibrium conditions to minimize the potential effect of kinetics on the isotopic fractionation. The experiments were performed within experimental series consisting of two steps as described below.

2.2.2. Starting materials

All experiments were performed using Alfa Aeser® 100 mesh hydrated silicic acid powder (SiO_2,am powder). Ultrafine particles were removed from the powder by sedimentation using the approach of Pokrovski and Schott (1998). Specifically, 50 g of the powder was suspended in >18.2 Ω de-ionized Milli-Q® water by stirring in a 1dm^3 glass beaker. The solid was sedimented and then the fluid phase decanted. This was repeated until the supernatant became clear within the first 5 min. The powder was subsequently oven dried, and placed into a desiccator while cooling.

Two aqueous solutions, one containing 0.05 mol/kg and the other 0.08 mol/kg catechol were prepared by dissolving Merck® pyrocatechol ($C_6H_4(OH)_2$) into a NH_4Cl – NH_3 pH-buffer solution. The buffer solution was prepared from de-ionized Milli-Q® water, suprapur Merck® NH_4Cl salt and Merck® 25 % NH_3 solution and contained 0.1 mol/kg NH_4Cl and 0.36 mol/kg NH_3.

2.2.3. Step 1: Equilibration of the reactive aqueous solutions with amorphous SiO_2.

Experiments in this study were performed within two distinct series. One series was performed with an aqueous 0.05 mol/kg catechol solution and the other with a 0.08 mol/kg catechol solution prepared as described above. These solution compositions were chosen as they were likely to contain high percentages of Si bound in VI-coordinated aqueous complexes. Each aqueous solution (200 mL) was first equilibrated with 3 g of washed amorphous SiO_2 powder in a closed polypropylene (PP) bottle. The closed bottles were placed in a constantly shaking thermostatic bath at 25°C. The aqueous solutions were regularly sampled over 10 days. The short equilibration period was chosen as aqueous catechol decomposes or reacts with ammonia over time (Barnum, 1972). The pH and concentration of the aqueous solutions were measured immediately after sampling. The aqueous Si concentrations of the fluid samples were determined by colorimetry. When the measured pH, and the Si concentrations of the sampled solutions attained a constant value, chemical equilibrium was assumed to be reached. The equilibrated aqueous solutions were then filtered with Teflon syringe filters (Merck® 0.2 μm).

2.2.4. Step 2: Isotopic exchange experiments.

To employ the three-isotope method, the chemically equilibrated solutions were enriched with a small quantity of ^{29}Si isotope tracer solution having an initial composition of 0.21% ^{28}Si, 99.76% ^{29}Si, and 0.03% ^{30}Si, to obtain starting reactive fluids having a $\delta^{29}Si$ ~23‰. To ensure that these fluids were still at equilibrium with SiO_2,am after adding the spike, the pH and Si concentrations of these spiked fluids were measured. The isotope exchange experiments in this study were conducted in two series consisting of 8 individual closed system experiments and lasted up to 7 days. The short duration of the experiments avoids the decomposition of the aqueous catechol. By performing individual closed system experiments, solids and fluids could be collected and analysed after selected experiment

durations. For the individual experiments, ~0.30 g of freshly pre-washed SiO_2,am powder with a known Si isotope composition was placed in 10 ml polypropylene reactors together with 10 ml of the prepared ^{29}Si enriched aqueous catechol solution. The reactors were wrapped in aluminium foil, to avoid light, and placed in an orbital shaker to be constantly mixed at 25 °C. To verify that the reactors were indeed closed, they were weighted at the beginning and end of each experiment. The experiments were terminated at pre-chosen times. Once an experiment was complete, the reactor was centrifuged for 20 min at 4500 rpm. The supernatant was then separated from the powder and filtered with Merck® 0.2 µm Teflon syringe filters. The pH and Si concentrations of the recovered aqueous solutions were measured just after sampling. These solutions were then immediately prepared for column chromatography to avoid any isotopic fractionation during decomposition of the organic ligand. The powders were washed and filtered with de-ionized Milli-Q® water, oven dried at 40°C, then stored prior to Si isotopic analysis.

2.3. Analytical methods

2.3.1. Characterization of SiO_2 powder

The cleaned SiO_2,am powder, and the SiO_2,am powder collected from the longest duration experiments were characterized using a JEOL JSM-7800F Prime scanning electron microscope (SEM) and a JEOL JEM-ARM200F Cold FEG transmission electron microscope (TEM) , both located at the Raimond Castaing Microcharaterization Centre (Toulouse, France). Some representative images are shown in Fig. 2. The average grain size of the cleaned silicic acid powder was 23 ± 7 nm (n=100, S.D.) as determined using TEM images and the ImageJ software package (Schindelin et al., 2012). The water content of the powder was determined to be 7.86 % by thermogravimetric analysis using a Mettler Toledo® ATG/DSC1. This is consistent with the chemical formula $SiO_2 \bullet 0.28\ H_2O$.

232 The specific surface area of the cleaned amorphous SiO_2 powder used in the
233 experiments was determined to be 195.6 m^2/g with an estimated uncertainty of ± 10% using
234 a Quantachrome Autosorb-1MP, together with the nitrogen multipoint BET method
235 (Brunauer et al., 1938).
236
237 **2.3.2. Characterization of aqueous solutions.**
238 The pH of all aqueous solutions was determined using a Metrohm® 913 pH Meter
239 connected to a standard glass microelectrode. The electrode was calibrated using certified
240 Orion Thermo Scientific® buffers, and yielded an uncertainty of 0.05 pH unit (2 SD).
241 Aqueous silicon concentrations were determined by the molybdate blue method
242 (Truesdale and LeCorre, 1975) using a Bran & Luebbe® analyser-III colorimeter coupled to
243 a Seal XY-2 autosampler and a Technicon analyser II mixing unit. The Si concentrations of
244 the measurements ranged from 0.1 to 10 ppm, with a long-term reproducibility within 3%
245 and a quantification limit of 0.04 ppm. To exclude possible uncertainties in measured Si
246 concentrations introduced by the presence of catechol, aqueous solutions with known Si
247 concentration were prepared, doped with 0.05 M and 0.08 M catechol, and measured at the
248 same time as the experimental solutions. No effect of the presence of aqueous catechol was
249 observed in the analyses.
250 ^{29}Si nuclear magnetic resonance (NMR) was used to verify the presence of the Si-
251 catecholate ($SiCat_3^{2-}$) complex in the aqueous solutions. Two 1.8 mM ^{29}Si solutions were
252 prepared, one at pH = 10.1 without catechol and the second at pH = 8.9 with a catechol
253 concentration of 0.05 mol/kg to match the experiments. In NMR glass tubes, 300 µl of the
254 ^{29}Si solutions were mixed with 300 µl D_2O as a solvent. NMR measurements were carried
255 out at 298K using a Bruker® AVANCE III HD 500 spectrometer at the ICT Institut de
256 Chimie in Toulouse. The spectrometer was set at 11.7 T and a resonating frequency of 99.35
257 MHz for ^{29}Si using a 5 mm Z-gradient BBO Prodigy cryoprobe. The ^{29}Si NMR chemical

shifts are reported in ppm relative to the $SiMe_4$ internal standard. An echoing pulse program (spin-echo for X nuclei with 1 H inverse gated decoupling) was used with a relaxation delay of 20s. The acquisition time for the solution without catechol was 0.5 h with 96 scans, whereas the acquisition time for the catechol was 17.75 h with 3072 scans.

2.3.3. Data reporting and Si isotope analysis

Silicon isotope compositions were measured on all aqueous solutions and solids sampled from the isotope exchange experiments, as well as the initial soild, the non-spiked chemically equilibrated aqueous solutions, and the spiked initial aqueous solutions. The silicon isotope compositions in this study are expressed using the standard δ-notation in per mil (‰) relative to the international NBS-28 standard (NIST RM-8546) as defined by:

$$\delta^{x}\mathrm{Si} = \left[\frac{(^{x}\mathrm{Si}/^{28}\mathrm{Si})_{sample}}{(^{x}\mathrm{Si}/^{28}\mathrm{Si})_{NBS-28}} - 1\right] \times 1000 \quad (4)$$

where *x* denotes the mass of Si, either ^{29}Si or ^{30}Si, and $(^{x}\mathrm{Si}/^{28}\mathrm{Si})_{sample}$ refers to the molar ratio of the Si with mass *x* to that of mass 28 in the sample.

The fractionation between an aqueous fluid and a solid ($\alpha^{x/28}_{fluid-solid}$) is defined either as

$$\alpha^{x/28}_{fluid-solid} = \frac{(^{x}\mathrm{Si}/^{28}\mathrm{Si})_{fluid}}{(^{x}\mathrm{Si}/^{28}\mathrm{Si})_{solid}} \quad (5)$$

or as

$$\Delta^{x}\mathrm{Si}_{fluid-solid} = \delta^{x}\mathrm{Si}_{fluid} - \delta^{x}\mathrm{Si}_{solid} \quad (6)$$

Note that $\Delta^{x}\mathrm{Si}_{fluid\text{-}solid}$, is approximately related to $\alpha^{x/28}_{fluid-solid}$ by Eqn. (2).

The uncertainty in retrieved Si isotope fractionation factors is calculated from the error propagation function given by

$$E\Delta^{x}\mathrm{Si}_{fluid-solid} = [(E\delta\,^{x}Si_{fluid})^{2} + (E\delta\,^{x}Si_{solid})^{2}]^{1/2} \quad (7)$$

where $E\Delta^{x}Si_{fluid\text{-}solid}$ is the uncertainty of the Si isotope fractionation factor, and $E\delta^{x}Si_{fluid}$ and $E\delta^{x}Si_{solid}$ are the analytical error of the indicated analysis of the fluid and solid, respectively. Note that uncertainties due to the extrapolation of Si compositions to 100% of isotope exchange are taken into account.

To determine their isotopic compositions, SiO_2,am powders were prepared by an initial calcination of 1-5 mg of each powder at 500 °C (Cornu et al., 1999) and then using the alkali fusion method of Zambardi and Poitrasson (2011). The sampled aqueous solutions were prepared for isotope analysis by a combination of calcination, similar to the approach of Cornu et al. (1999) for soils, and the alkali fusion method of Zambardi and Poitrasson (2011). In detail, five ml of aqueous solution was evaporated in silver crucibles (XRF scientific, Montreal, Canada). The remaining Si and organic residue were then calcined by heating the crucibles in a furnace at 500°C for 4h, destroying all remaining organic residue, leaving only the Si of the solution behind. After cooling, ~200 mg of Merck® NaOH pellets were weighted into the crucibles. The crucibles were capped and placed into a furnace heated at 720°C for 10 min. After cooling to room temperature, the crucibles were placed into 30 ml Savillex® Teflon beakers filled with 15 ml Milli-Q® water to dissolve the amorphous SiO_2 powder. The resulting aqueous solutions were transferred after 24 hours into 30 mL polypropylene bottles and diluted with Milli-Q® water to 20 ml and subsequently acidified with ~10 N bi-distilled HCl to a pH of 1.5.

All samples were purified prior to Si isotope analysis by cation exchange chromatography using 2 ml of Bio-Rad® AG50W-12X cationic resin filled into 10 ml Bio-Rad® polypropylene columns. The resin was initially cleaned as described in Georg et al. (2006). After cleaning, 2 ml of the liquid samples were loaded onto the column, directly collected, and eluted twice with 2 ml Milli-Q® water. The collected fluids were then diluted and acidified to obtain a 3 ppm Si solution and a total HCl concentration of 0.05 mol/kg. The overall Si recovery was determined to be between 90 and 100 %. The ^{28}Si signal of the

306 procedural blank was found to be less than 3% of the total signal, which can be considered
307 negligible. This was confirmed by assuming a signal bias of 3%, within a -1‰ to +1‰
308 signature range as shown in Supplemental Table B.2. For the solids, the maximum bias
309 effect on the isotopic signature is < 0.04 ‰, which is four times less than the measured 2 SD
310 uncertainty.

311 Silicon isotope ratios were determined using the Thermo Scientific Neptune® MC-
312 ICP-MS located at the Laboratore Géosciences Environnement Toulouse (GET), France.
313 Measurements were performed under wet plasma conditions in medium resolution. A
314 Thermo SIS system was used together with a double-pass cyclonic spray chamber to inject
315 the samples into the spectrometer. Instrumental mass bias drift was corrected using sample-
316 standard bracketing combined with Mg addition as an internal standard. Measurements of
317 $^{25}Mg/^{24}Mg$ ratios were performed in the dynamic mode. Russell's exponential law (Russell
318 et al., 1978) was used to further correct for the mass bias drift.

319 To ensure the accuracy and precision of the isotopic analysis, the BHVO-2 reference
320 material was repeatedly measured during each run. The results yielded $\delta^{30}Si = -0.25 \pm$
321 0.16 ‰, and $\delta^{29}Si = -0.13 \pm 0.08$ ‰ (2 S.D, n=48), which is in close agreement with the
322 measured BHVO-2 values of Savage et al. (2014).

323

324 **3. Results**

325 **3.1. First-principle calculations of equilibrium fractionation factors**

326 To assess the role of changing Si coordination due to aqueous organic complexation
327 on its isotope fractionation properties, both VI-fold and V-fold coordination compounds
328 were considered (see Methods). A goal of this study was to determine the Si isotope
329 fractionation of these compounds relative to amorphous silica, the predominant naturally
330 forming Si-oxide solid formed at ambient temperature. The modeling of amorphous silica,
331 however, is difficult because its structure and composition, in particular its degree of

hydration is poorly defined. The Si equilibrium fractionation factors were thus calculated between these species and either quartz or dissolved $H_4SiO_4^0$, which represent two compositional end-members of amorphous silica. The quality of isotopic predictions based on DFT depend on the accuracy of the calculated frequencies. For a large number of ^{IV}Si materials, it was shown that PBE functionals underestimate frequencies by 5%, leading to a 5-10% underestimation of Si fractionation properties depending on temperature (Méheut et al., 2009). The resulting uncertainties for quartz are discussed in Supplemental Information A for both the PBE and vdW-DF2 functionals. Results show that the fractionation properties of quartz calculated using either functional yield nearly identical results. The compounds considered in these calculations other than quartz, are molecular crystals where weak dispersion forces play an important role differently from previous calculations on silicate minerals (Méheut et al., 2007, 2009; Méheut and Schauble, 2014; Huang et al., 2014). Previous calculations were based on the PBE (Perdew et al., 1996) or LDA (Perdew and Zunger, 1981) functionals, which by their construction essentially miss dispersion effects. Improved functionals, meant to better account for dispersion, have been designed to account for these effects. Notably, the vdW-DF2 non-local functional (Lee et al., 2010) was also considered in this study. The calculated Si isotope fractionation of investigated compounds relative to quartz is plotted as a function of Si-O bond distance in Fig. 3. This figure shows that the vdW-DF2 functional, designed to take into account dispersion forces better than PBE, gives identical Si-O distances, but slightly larger Si isotope fractionations with respect to quartz. As discussed in Supplemental Information A, it is difficult to verify the relative accuracy of the vdW-DF2 functional owing to the lack of comparable direct measurements. Consequently, the difference between the results obtained using the two functionals were used to estimate the error of these calculations. Resulting calculations give at 25 °C $\Delta_{eq}{}^{30}Si_{SiCat_3{}^{2-}\text{-}quartz}$ = -21.9±1.2 ‰, $\Delta_{eq}{}^{30}Si_{SiDio\text{-}quartz}$ = -11.7±0.6 ‰, $\Delta_{eq}{}^{30}Si_{SiGly\text{-}quartz}$ = -11.7±0.9 ‰, $\Delta_{eq}{}^{30}Si_{SiLact\text{-}quartz}$ = -12.2±0.7 ‰. The equations describing these fractionations

as a function of temperature are listed in Table 1. Combining these values with values of the silicic acid-quartz equilibrium Si isotopes fractionation (Dupuis et al., 2015) $\Delta_{eq}{}^{30}Si_{H_4SiO_4{}^0\text{-}quartz}$= -2.10 ‰ at 25 °C, provides the following Si isotope equilibrium fractionation factors among these compounds and aqueous silicic acid: $\Delta_{eq}{}^{30}Si_{SiCat_3{}^{2}\text{-}H_4SiO_4{}^0}$ = -19.8±1.2 ‰ and $\Delta_{eq}{}^{30}Si_{SiDio\text{-}H_4SiO_4{}^0}$= -9.6±0.6 ‰ (see Fig. 4).

3.2. Experimentally determined equilibrium Si isotope fraction factors between aqueous silicic acid and the aqueous Si-catecholate complex

The results of first-principle calculations described above suggest a large Si isotope fractionation due to aqueous Si-organic ligand complexing. To validate the results of these first-principle calculations, isotope exchange experiments at bulk chemical equilibrium were performed to measure the equilibrium Si isotope fraction factor between aqueous silicic acid ($H_4SiO_4{}^0$) and the aqueous Si-catecholate complex ($SiCat_3{}^{2-}$). The presence of the aqueous Si-catecholate complex was confirmed by NMR measurements. The spectra of two representative 1.8 mM silica solutions are shown in Supplemental Fig. B.1a and b. The NMR spectrum of the solution containing 0.05 mol/l catechol shows a clear shift of the ^{29}Si peak to 144.2 ppm, compared to 72.3 ppm in the catechol-free solution. This confirms that silicon is mainly present in the form of the VI-coordinated Si-catecholate anion in the solution containing 0.05 mol/l catechol.

In the first step of the experiments, the reactive aqueous solutions were chemically equilibrated with pre-washed amorphous SiO_2,am powder.. The chemical evolution of these fluids during this first equilibration step can be seen in the Supplemental Table B.2. After attainment of SiO_2,am-fluid chemical equilibrium, the solids and fluids were separated and a ^{29}Si spike was added to the fluid. Some of the original pre-washed SiO_2,am powder was added to the spiked fluid, which was then in chemical equilibrium but isotopic

383 disequilibrium with the amorphous SiO_2 powder. For each series, 8 individual closed system
384 experiments were prepared, and stopped after pre-chosen time intervals (Table 2).

385 The water content of the silica powder recovered from the longest experiments of
386 each series decreased slightly from 7.86 % to 6.54 %. The grain size of the solids did not
387 change but their BET surface area was 10-15 % lower than that of the pre-experiment
388 powder. These changes could result from some minor Ostwald ripening of the amorphous
389 silica grains during the experiments; however, the post experiment solids appear unchanged
390 by the isotope exchange experiments under scanning electron microscope (SEM) and
391 transmission electron microscope (TEM). Representative images are shown in Fig.2.

392 The pH and Si concentration of the aqueous 0.05 mol/kg catechol fluid remained
393 constant during the isotope exchange experiments as shown in Fig. 5. The aqueous 0.08
394 mol/kg catechol experiments however, show an initial decrease of pH from 8.9 to 8.7, and a
395 decrease in dissolved Si concentration of 9%, but this stabilised after 6 hours. The longest
396 duration experiment of the 0.05 and 0.08 mol/kg catechol experiment series showed a
397 decrease of ~ 10% in dissolved Si concentration likely due to slight catechol oxidation.
398 These two fluids were not considered in the retrieval of equilibrium isotope fractionation
399 factors.

400 The temporal evolution of the Si isotopic compositions of the aqueous fluids and
401 solids during the two 7-day of isotopic exchange experimental series are shown in Fig. 5. In
402 both experimental series, the $\delta^{29}Si$ values of the fluids and solids shown in Fig. 5 a and b
403 mirror one another consistent with Si isotope exchange at bulk chemical equilibrium. The
404 ^{29}Si concentrations of the enriched fluids decrease rapidly during the first 3h and the
405 corresponding $\delta^{29}Si$ value of the solids increase. A similar trend is exhibited by the $\delta^{30}Si$
406 values shown for both experiments in Fig. 5. All chemical and isotopic compositions of the
407 fluids and solids are listed in Table 2.
408

3.3. Retrieval of silicon equilibrium isotope fractionation factors

To determine the equilibrium fractionation factors between the experimental fluids and the SiO_2,am powder ($\Delta_{eq}{}^{30}Si_{fluid\text{-}SiO_2,am}$), the isotopic compositions $\delta^{30}Si$ of the fluids and the amorphous silica powder were first plotted as a function of the degree of isotopic exchange, *F*, (see the materials and methods section for details) as shown in Fig 6. *F* values range from 0 to 1, where 1 indicates that 100 % of the isotopes are exchanged between fluid and SiO_2,am powder, and isotopic equilibrium is reached. It can be seen that at the end of the experimental series, from 60 to 70 % of the equilibrium fractionation value was attained (Fig. 6 a and b). The three-isotope method allows the determination of the equilibrium fractionation factor $\Delta_{eq}{}^{30}Si_{fluid\text{-}SiO_2,am}$, by extrapolation of the isotopic compositions of the fluid and SiO_2,am to F=1 (Matthews et al., 1983). The overall $\Delta_{eq}{}^{30}Si_{fluid\text{-}SiO_2,am}$ generated from the experiments performed in this study from the experimental series run in the 0.05 mol/kg catechol solutions was -16.38 ± 1.71 ‰, and that obtained from the experiments run in the presence of 0.08 mol/kg catechol was -18.01 ± 3.43 ‰.

The equilibrium fractionation factor between the fluid and amorphous silica is the weighted sum of the equilibrium fractionation factors between the Si aqueous species present in the solution and amorphous silica (see Eqn. 1). In the experiments performed in this study, silicic acid and the Si-catecholate complex ($SiCat_3^{2-}$) were the only Si aqueous species present in solution as shown by the results of speciation calculations with the PHREEQC code (Parkhurst and Appelo, 2013) listed in Table 3. The equilibrium Si isotope fractionation between $SiCat_3^{2-}$ and $H_4SiO_4^0$, $\Delta_{eq}{}^{30}Si_{SiCat_3^{2-}\text{-}H_4SiO_4^0}$, could therefore be derived by modifying Eqn. 1 to

$$\Delta_{eq}{}^{30}Si_{fluid\text{-}SiO_2,am} = x_{H_4SiO_4^0}\,\Delta_{eq}{}^{30}Si_{H_4SiO_4^0\text{-}SiO_2,am} + x_{SiCat_3^{2-}}\,\Delta_{eq}{}^{30}Si_{SiCat_3^{2-}\text{-}SiO_2,am} \quad (8)$$

and

$$\Delta_{eq}{}^{30}Si_{SiCat_3^{2-}\text{-}H_4SiO_4^0} = \Delta_{eq}{}^{30}Si_{SiCat_3^{2-}\text{-}SiO_2,am} - \Delta_{eq}{}^{30}Si_{H_4SiO_4^0\text{-}SiO_2,am} \quad (9)$$

where x_i stands for the mole fraction of the *i*th aqueous Si species. Using the equilibrium isotope fractionation factors between the fluid and SiO_2,am determined in this study and between $H_4SiO_4^0$ and SiO_2,am determined by Stamm et al. (2019), the equilibrium fractionation factor between $SiCat_3^{2-}$ and $H_4SiO_4^0$, $\Delta_{eq}{}^{30}Si_{SiCat_3^{2-}\text{-}H_4SiO_4 0}$, can be derived for both catechol fluids (see Table 3). Taken together they provide an equilibrium isotope fractionation factor between the $SiCat_3^{2-}$ and $H_4SiO_4^0$ aqueous species, $\Delta_{eq}{}^{30}Si_{SiCat_3^{2-}\text{-}H_4SiO_4 0}$ of -18.69 ± 0.49 ‰. This value is in close agreement with that determined with the first-principle calculations as shown in Fig. 4.

4. Discussion

4.1. Effect of aqueous Si coordination on its fractionation properties: First-principle calculations

Figure 3 shows the relationship between the coordination of the Si species, its mean Si-O bond distance ($\overline{d}_{Si\text{-}O}$) and the computed equilibrium Si isotopic fractionation with respect to quartz. This relationship was previously discussed for the case of compounds containing IV-fold Si (Méheut and Schauble, 2014; Dupuis et al., 2015). Here, a regression based on IV, V and VI coordination (see Fig. 3 caption) leads to:

$$\Delta^{30}Si_{silicate\text{-}qtz}\,(\text{at } 300^{o}K) = -113*(\overline{d}_{Si\text{-}O} - 1.626) \quad (3)$$

4.2. Equilibrium Silicon isotope fractionation in the presence of catechol.

The first-principle calculations and the experiments performed in this study verify an extreme equilibrium Si isotope fractionation in the presence of the organic ligand catechol. The 25 °C calculated equilibrium isotope fractionation factor between the aqueous Si-catecholate complex ($SiCat_3^{2-}$) and silicic acid ($H_4SiO_4^0$) is -19.8 ± 1.2 ‰ at 25 °C while the

experimental value was determined to be -18.69 ± 0.49 ‰. This contrasts with the relatively small 25 °C equilibrium isotopic fractionation factors observed between the two major naturally forming aqueous inorganic Si species $H_3SiO_4^-$ and $H_4SiO_4^0$; values of $\Delta_{eq}{}^{30}Si_{H_3SiO_4^- - H_4SiO_4^0}$ range from -1.60 ± 0.30 ‰ to -2.34 ± 0.13 ‰ (Dupuis et al., 2015; Stamm et al., 2019). In each case silicic acid is enriched in the heavier ^{30}Si isotope, but this fractionation is far greater in the presence of the aqueous Si-catecholate complex ($SiCat_3^{2-}$). This large increase in Si equilibrium isotope fractionation is due to the increase in the aqueous Si coordination number from IV to VI, and the resulting increase of the Si-O bond length (~1.645 Å for Si(IV) versus ~1.815 Å for Si(VI)) due to the addition of catechol to the aqueous solution. Note, that the amount of catechol used in our experiments is far higher than that typically found in nature. Nevertheless, even a small concentration of catechol or any organic ligand forming with Si organosilicon complexes containing hexaoxo-silicon sites can have a significant effect on the equilibrium fractionation factors between aqueous Si and co-existing solid phases. This is because the overall fractionation of an element between a fluid and an aqueous phase depends on the mole fraction weighted distributed speciation in the aqueous phase (see Eqn. 1).

The formation of aqueous V-fold coordinated silicon species with aliphatic sugar acids or polyhydroxy alcohols has been demonstrated in previous studies (Kinrade et al., 1999, 2001a, 2001b). The equilibrium isotopic fractionation factors associated with such pentaoxo-silicon coordination have not yet been investigated experimentally. However, the first principle calculations performed in this study suggest that the equilibrium fractionation factor between a V-fold coordinated aqueous Si complex and $H_4SiO_4^0$ is -9.9 ‰, which is approximately half of the corresponding fractionation between VI-fold coordinated Si and $H_4SiO_4^0$.

4.3. Implications for biosilicification

Silicon is an essential element in the biomineralization i.e. biosilicification processes. When dissolved Si is absorbed into organisms, the proteinaceous matrices within these organisms can facilitate the precipitation of Si and thus the mineral growth (Perry, 2003). Enzymes and proteins play an important role in the secretion of silica skeletal structures of marine organisms such as sponges, choanoflagellates and diatoms, enhancing their growth rate (Otzen, 2012). The extent to which aqueous Si is transported and complexed by the enzymes and proteins involved in the building of these skeletal structures is still poorly known, and thus the impact of these on the isotopic fractionation is not well constrained (Wang et al., 2019).

Diatoms are siliceous algae, and one of the main silicifying organisms in the modern ocean (Otzen, 2012). They exhibit an isotope fractionation factor of -1.1 ‰; this is considered to be influenced by either a Rayleigh or a steady-state isotope fractionation mechanism (e.g. Frings et al., 2016). Even lighter Si isotope compositions are found in sponges. An isotope fractionation up to -6.5 ‰ has been measured between seawater and sponge spicules (e.g. Wille et al., 2010; Cassarino et al., 2018). Equally light Si isotope compositions, values as low as -7 ‰, were found in cultured choanoflagellates, the sister taxon of sponges (Marron et al., 2019). The strong fractionations observed in sponges and choanoflagellates, which are inconsistent with Rayleigh distillation (Wille et al., 2010; Cassarino et al., 2018), could be attributed to the silica uptake into the cell or to the silicification process. Although little is known about Si uptake at the atomic level, it is generally agreed that the silicification of these two taxa involves an enzymatic reaction obeying Michaelis-Menten kinetics (Wille et al., 2010; Hendry and Robinson, 2012; Cassarino et al., 2018).

Two major steps could affect Si isotope fractionation during biomineralization: i) Si transport across the cell membrane by active or passive membrane proteins (Marron et al.,

2019) or via a sodium transporter leading to high intracellular Si concentrations (i.e. NBCSA; Schröder et al., 2008; Otzen, 2012), and ii) Si polymerization within the cell, associated with an organic template (Milligan et al., 2004; Tesson et al., 2017). Based on such schemes, it has been proposed that Si could undergo kinetic fractionation during its transport across the cell membrane and internally during spicule formation (Milligan et al., 2004; Wille et al., 2010; Cassarino et al., 2018). In particular, Wille et al. (2010) advocated that substantial Si isotopic fractionation could occur during the transport between high Si influx into the cell and the efflux of excess Si out of the cell.

The results of this study suggest an impact of aqueous organic Si speciation on bio-silica precipitation mechanisms. After silicon uptake into the cell, Si precipitation, which occurs in the axial canal of the central filament of the spicule, is controlled by enzymes such as silicatein or glassin, which promotes both silicase (silica solubilisation) and condensation reactions (e.g. Perry, 2003). The mechanism of Si condensation mediated by silicatein has been proposed to involve the interaction of the putative active site serine-26 and histidine-165 site chains leading to the formation of a transitory intermediate where pentavalent Si is stabilized through a donor bond from the imidazole nitrogen atom (Zhou et al., 1999; Kinrade et al., 2002). In the absence of further interaction with silicic acid, the light isotope signature resulting from V-fold aqueous Si complexing with these organics could be preserved and therefore could contribute to the large isotopic fractionation observed between seawater and the sponge spicules. Differences in Si isotope fractionation of sponges and diatoms could be explained by the different biomolecules the organisms use to incorporate Si into their structures. Diatoms use silaffins and silacdins to form their biosilicate frustules (Marron et al., 2019).

Plants, like sponges and diatoms, preferentially incorporate light Si isotopes into their structure (e.g. Opfergelt et al., 2006). However, the biochemistry of Si in plants is not well known, Lsi2 genes were identified as having a role in silicon transport (Marron et al.,

537 2019). Kinrade (1999) suggested that the Si transport may not occur as $H_4SiO_4^0$ through
538 plants, but as hypercoordinated organosilicon complexes formed by silicon with phenols or
539 carbohydrates molecules containing at least four adjacent hydroxyl groups. Si-enterobacti, a
540 complex of the siderophore enterobactin, where Si is hexacoordinated, has been isolated
541 from an endophytic *Streptomyces sp*. occurring in *Piper guinensis* (Kenla et al., 2013). The
542 results presented in this study suggest that the presence of even a small concentration of
543 hypercoordinated organosilicon complexes would lead to a strong negative fractionation
544 between the fluid phase and Si incorporated in the plant structure.

545 As aqueous Si complexation alters the fractionation of this metal into solids, and as
546 aqueous ligands are abundant in various organisms, it seems reasonable to conclude that
547 insight into the biosilicification process would be gained from the Si isotopic compositions
548 of biomaterials. The results in this study show that both rigorous experiments and detailed
549 first-principle calculations can aid in this effort.

550

551 **5. Conclusions**

552 The results of this study demonstrate that the formation of organosilicon complexes
553 containing aqueous pentaoxo- and hexaoxo- silicon species rather than the IV-coordinated Si
554 centres typical of most aqueous silica species can have a large influence on the equilibrium
555 Si isotope fractionation between fluids and Si-bearing solids. Indeed, the study has shown
556 that the isotopic composition of the aqueous hexaoxo-$SiCat_3^{2-}$ complex is about 19 ‰ lighter
557 than that of aqueous silicic acid at ambient temperature. This value, which is far larger than
558 ever previously measured for Si fractionation between a natural solid and its coexisting
559 aqueous fluid is in close agreement with the results of the first-principle calculations
560 performed in this study demonstrating the robustness of both type of Si isotope
561 quantifications. Note that the Si isotope composition of organosilicon complexes containing
562 pentaoxo-silicon is calculated for the Si-diolate, Si-glyconate and Si-methyllactate systems

to be about 10 ‰ lighter than that of silicic acid. Such results demonstrate that the presence of aqueous organic ligands in natural systems can play an important role on the Si isotopes fractionation and thus might explain the strong negative fractionation found in numerous biological systems.

Acknowledgements

This research was funded by ISONOSE a People Programme (Marie Curie Actions) of the European Unions' Seventh Framework Programme FP7/2017-2013/ under REA grant agreement n° [608069]. This work was performed using HPC resources from CALIMP (Calcul eb Midi-Pyrénées; Grant 2017-P1037). The authors acknowledge Gwénaëlle Guittier from the Laboratoire de Génie Chimique (INP-ENSIACET) for TGA measurements, Philippe De Parseval, and Teresa Hungria from the Centre de MicroCaractérisation Raimond Castaing for SEM and TEM measurements, and Marc Vedrenne from the Institut de Chimie de Toulouse (ICT) for NMR measurements. Furthermore, the authors thank Alain Castillo, Carole Causserand, and Manuel Henry from the Géosciences Environement Toulouse for their assistance in the laboratories. Kate Hendry from the University of Bristol is acknowledged for her input on biosilicification. François-Xavier d'Abzac, Anna Harrison, Chiara Marieni, Moritz Lissner, Giuseppe Saldi, and Martin Voigt are acknowledged for constructive discussions, and contributions to this work. This work has benefited for the insightful comments of two anonymous reviewers.

583 **References**

584 Balan, E., Noireaux, J., Mavromatis, V., Saldi, G.D., Montouillout, V., Blanchard, M.,
585 Pietrucci, F., Gervais, C., Rustad, J.R., Schott, J., Gaillardet, J., 2018. Theoretical
586 isotopic fractionation between structural boron in carbonates and aqueous boric acid
587 and borate ion. Geochim. Cosmochim. Acta 222, 117–129.
588 https://doi.org/10.1016/j.gca.2017.10.017
589 Baldereschi, A., 1973. Mean-Value Point in the Brillouin Zone. Phys. Rev. B 7, 5212–5215.
590 https://doi.org/10.1103/PhysRevB.7.5212
591 Barnum, D.W., 1972. Reaction of catechol with colloidal silica and silicic acid in aqueous
592 ammonia. Inorg. Chem. 11, 1424–1429. https://doi.org/10.1021/ic50112a052
593 Barnum, D.W., 1970. Catechol complexes with silicon. Inorg. Chem. 9, 1942–1943.
594 https://doi.org/10.1021/ic50090a038
595 Baroni, S., de Gironcoli, S., Dal Corso, A., Giannozzi, P., 2001. Phonons and related crystal
596 properties from density-functional perturbation theory. Rev. Mod. Phys. 73, 515–
597 562. https://doi.org/10.1103/RevModPhys.73.515
598 Benner, K., Klüfers, P., Schuhmacher, J., 1999. Diolato-silicat- und -germanat-Ionen aus
599 wäßrig-alkalischer Lösung. Z. Für Anorg. Allg. Chem. 625, 541–543.
600 https://doi.org/10.1002/(SICI)1521-3749(199904)625:4<541::AID-
601 ZAAC541>3.0.CO;2-A
602 Benner, K., Klüfers, P., Vogt, M., 2003. Hydrogen-Bonded Sugar-Alcohol Trimers as
603 Hexadentate Silicon Chelators in Aqueous Solution. Angew. Chem. Int. Ed. 42,
604 1058–1062. https://doi.org/10.1002/anie.200390274
605 Bigeleisen, J., Mayer, M.G., 1947. Calculation of Equilibrium Constants for Isotopic
606 Exchange Reactions. J. Chem. Phys. 15, 261–267. https://doi.org/10.1063/1.1746492
607 Brunauer, S., Emmett, P.H., Teller, E., 1938. Adsorption of Gases in Multimolecular Layers.
608 J. Am. Chem. Soc. 60, 309–319. https://doi.org/10.1021/ja01269a023
609 Cassarino, L., Coath, C.D., Xavier, J.R., Hendry, K.R., 2018. Silicon isotopes of deep sea
610 sponges: new insights into biomineralisation and skeletal structure. Biogeosciences
611 15, 6959–6977. https://doi.org/10.5194/bg-15-6959-2018
612 Cella, J.A., Cargioli, J.D., Williams, E.A., 1980. 29Si NMR of five- and six-coordinate
613 organosilicon complexes. J. Organomet. Chem. 186, 13–17.
614 https://doi.org/10.1016/S0022-328X(00)93813-0
615 Cornu, S., Lucas, Y., Lebon, E., Ambrosi, J.P., Luizão, F., Rouiller, J., Bonnay, M., Neal,
616 C., 1999. Evidence of titanium mobility in soil profiles, Manaus, central Amazonia.

Geoderma 91, 281–295. https://doi.org/10.1016/S0016-7061(99)00007-5

Dal Corso, A., 2014. Pseudopotentials periodic table: From H to Pu. Comput. Mater. Sci. 95, 337–350. https://doi.org/10.1016/j.commatsci.2014.07.043

Donhärl, W., Elhofer, I., Wiede, P., Schubert, U., 1998. Elemental silicon and solid SiO give the same products as SiO_2 upon reaction with alkali-metal glycolates. J. Chem. Soc. Dalton Trans. 0, 2445–2446. https://doi.org/10.1039/A803672A

Dupuis, R., Benoit, M., Nardin, E., Méheut, M., 2015. Fractionation of silicon isotopes in liquids: The importance of configurational disorder. Chem. Geol. 396, 239–254. https://doi.org/10.1016/j.chemgeo.2014.12.027

Frings, P.J., Clymans, W., Fontorbe, G., De La Rocha, C.L., Conley, D.J., 2016. The continental Si cycle and its impact on the ocean Si isotope budget. Chem. Geol. 425, 12–36. https://doi.org/10.1016/j.chemgeo.2016.01.020

Füger, A., Méheut, M., Mavromatis, V., Leis, A., Dietzel, M., 2018. Oxygen isotope fractionation during smithsonite formation from aqueous solutions. Chem. Geol. 495, 76–89. https://doi.org/10.1016/j.chemgeo.2018.08.005

Georg, R.B., Reynolds, B.C., Frank, M., Halliday, A.N., 2006. New sample preparation techniques for the determination of Si isotopic compositions using MC-ICPMS. Chem. Geol. 235, 95–104. https://doi.org/10.1016/j.chemgeo.2006.06.006

Giannozzi, P., Baroni, S., Bonini, N., Calandra, M., Car, R., Cavazzoni, C., Ceresoli, D., Chiarotti, G.L., Cococcioni, M., Dabo, I., Dal Corso, A., de Gironcoli, S., Fabris, S., Fratesi, G., Gebauer, R., Gerstmann, U., Gougoussis, C., Kokalj, A., Lazzeri, M., Martin-Samos, L., Marzari, N., Mauri, F., Mazzarello, R., Paolini, S., Pasquarello, A., Paulatto, L., Sbraccia, C., Scandolo, S., Sclauzero, G., Seitsonen, A.P., Smogunov, A., Umari, P., Wentzcovitch, R.M., 2009. QUANTUM ESPRESSO: a modular and open-source software project for quantum simulations of materials. J. Phys. Condens. Matter 21, 395502. https://doi.org/10.1088/0953-8984/21/39/395502

Hahn, F.E., Keck, M., Raymond, K.N., 1995. Catecholate Complexes of Silicon: Synthesis and Molecular and Crystal Structures of [Si(cat)2].cntdot.2THF and Li2[Si(cat)3].cntdot.3.5dme (cat = Catecholate Dianion). Inorg. Chem. 34, 1402–1407. https://doi.org/10.1021/ic00110a018

Hendry, K.R., Robinson, L.F., 2012. The relationship between silicon isotope fractionation in sponges and silicic acid concentration: Modern and core-top studies of biogenic opal. Geochim. Cosmochim. Acta 81, 1–12. https://doi.org/10.1016/j.gca.2011.12.010

651 Hohenberg, P., Kohn, W., 1964. Inhomogeneous Electron Gas. Phys. Rev. 136, B864–B871.
652 https://doi.org/10.1103/PhysRev.136.B864
653 Huang, F., Wu, Z., Huang, S., Wu, F., 2014. First-principles calculations of equilibrium
654 silicon isotope fractionation among mantle minerals. Geochim. Cosmochim. Acta
655 140, 509–520. https://doi.org/10.1016/j.gca.2014.05.035
656 Jugdaohsingh, R., Pedro, L.D., Watson, A., Powell, J.J., 2015. Silicon and boron differ in
657 their localization and loading in bone. Bone Rep. 1, 9–15.
658 https://doi.org/10.1016/j.bonr.2014.10.002
659 Kenla, T.J.N., Tatong, M.D.K., Talontsi, F.M., Dittrich, B., Frauendorf, H., Laatsch, H.,
660 2013. Si-enterobactin from the endophytic Streptomyces sp. KT-S1-B5 – a potential
661 silicon transporter in Nature? Chem. Commun. 49, 7641.
662 https://doi.org/10.1039/c3cc44437f
663 Kinrade, S.D., Del Nin, J.W., Schach, A.S., Sloan, T.A., Wilson, K.L., Knight, C.T.G.,
664 1999. Stable Five- and Six-Coordinated Silicate Anions in Aqueous Solution.
665 Science 285, 1542–1545. https://doi.org/10.1126/science.285.5433.1542
666 Kinrade, S.D., Gillson, A.-M.E., Knight, C.T.G., 2002. Silicon-29 NMR evidence of a
667 transient hexavalent silicon complex in the diatom Navicula pelliculosa. J. Chem.
668 Soc. Dalton Trans. 307–309. https://doi.org/10.1039/b105379p
669 Kinrade, S.D., Schach, A.S., Hamilton, R.J., Knight, C.T.G., 2001a. NMR evidence of
670 pentaoxo organosilicon complexes in dilute neutral aqueous silicate solutions. Chem.
671 Commun. 1564–1565. https://doi.org/10.1039/b104713m
672 Kinrade, S.D., Hamilton, R.J., Schach, A.S., Knight, C.T.G., 2001b. Aqueous hypervalent
673 silicon complexes with aliphatic sugar acids. J. Chem. Soc. Dalton Trans. 961–963.
674 https://doi.org/10.1039/b010111g
675 Kohn, W., Sham, L.J., 1965. Self-Consistent Equations Including Exchange and Correlation
676 Effects. Phys. Rev. 140, A1133–A1138. https://doi.org/10.1103/PhysRev.140.A1133
677 Kubicki, J.D., Heaney, P.J., 2003. Molecular orbital modeling of aqueous organosilicon
678 complexes: implications for silica biomineralization. Geochim. Cosmochim. Acta
679 67, 4113–4121. https://doi.org/10.1016/S0016-7037(03)00093-0
680 Lee, K., Murray, É.D., Kong, L., Lundqvist, B.I., Langreth, D.C., 2010. Higher-accuracy
681 van der Waals density functional. Phys. Rev. B 82, 081101(R).
682 https://doi.org/10.1103/PhysRevB.82.081101
683 Marron, A., Cassarino, L., Hatton, J., Curnow, P., Hendry, K.R., 2019. The silicon isotopic
684 composition of choanoflagellates: implications for a mechanistic understanding of

685 isotopic fractionation during biosilicification. Biogeodciences, 16 4805-4813
686 https://doi.org/10.5194/bg-2019-181
687 Matsuhisa, Y., Goldsmith, J.R., Clayton, R.N., 1978. Mechanisms of hydrothermal
688 crystallization of quartz at 250°C and 15 kbar. Geochim. Cosmochim. Acta 42, 173–
689 182. https://doi.org/10.1016/0016-7037(78)90130-8
690 Matthews, A., Goldsmith, J.R., Clayton, R.N., 1983. On the mechanisms and kinetics of
691 oxygen isotope exchange in quartz and feldspars at elevated temperatures and
692 pressures. Geol. Soc. Am. Bull. 94, 396. https://doi.org/10.1130/0016-
693 7606(1983)94<396:OTMAKO>2.0.CO;2
694 Méheut, M., Lazzeri, M., Balan, E., Mauri, F., 2009. Structural control over equilibrium
695 silicon and oxygen isotopic fractionation: A first-principles density-functional theory
696 study. Chem. Geol., Applications of non-traditional stable isotopes in high-
697 temperature geochemistry 258, 28–37.
698 https://doi.org/10.1016/j.chemgeo.2008.06.051
699 Méheut, M., Lazzeri, M., Balan, E., Mauri, F., 2007. Equilibrium isotopic fractionation in
700 the kaolinite, quartz, water system: Prediction from first-principles density-
701 functional theory. Geochim. Cosmochim. Acta 71, 3170–3181.
702 https://doi.org/10.1016/j.gca.2007.04.012
703 Méheut, M., Schauble, E.A., 2014. Silicon isotope fractionation in silicate minerals: Insights
704 from first-principles models of phyllosilicates, albite and pyrope. Geochim.
705 Cosmochim. Acta 134, 137–154. https://doi.org/10.1016/j.gca.2014.02.014
706 Milligan, A.J., Varela, D.E., Brzezinski, M.A., Morel, F.M.M., 2004. Dynamics of silicon
707 metabolism and silicon isotopic discrimination in a marine diatomas a function of
708 pCO 2. Limnol. Oceanogr. 49, 322–329. https://doi.org/10.4319/lo.2004.49.2.0322
709 Opfergelt, S., Cardinal, D., Henriet, C., André, L., Delvaux, B., 2006. Silicon isotope
710 fractionation between plant parts in banana: In situ vs. in vitro. J. Geochem. Explor.
711 88, 224–227. https://doi.org/10.1016/j.gexplo.2005.08.044
712 Otzen, D., 2012. The Role of Proteins in Biosilicification. Scientifica 2012, 1–22.
713 https://doi.org/10.6064/2012/867562
714 Parkhurst, D.L., Appelo, C.A.J., 2013. Description of input and examples for PHREEQC
715 version 3—A computer program for speciation, batch-reaction, one-dimensional
716 transport, and inverse geochemical calculations. U.S. Geological Survey Techniques
717 and Methods, book 6, chap. A43, p. 497.
718 Perdew, J.P., Burke, K., Ernzerhof, M., 1996. Generalized Gradient Approximation Made

719 Simple. Phys. Rev. Lett. 77, 3865–3868.
720 https://doi.org/10.1103/PhysRevLett.77.3865
721 Perdew, J.P., Zunger, A., 1981. Self-interaction correction to density-functional
722 approximations for many-electron systems. Phys. Rev. B 23, 5048–5079.
723 https://doi.org/10.1103/PhysRevB.23.5048
724 Perry, C.C., 2003. Silicification: The Processes by Which Organisms Capture and
725 Mineralize Silica. Rev. Mineral. Geochem. 54, 291–327.
726 https://doi.org/10.2113/0540291
727 Poitrasson, F., 2017. Silicon Isotope Geochemistry. Rev. Mineral. Geochem. 82, 289–344.
728 https://doi.org/10.2138/rmg.2017.82.8
729 Pokrovski, G.S., Schott, J., 1998. Experimental study of the complexation of silicon and
730 germanium with aqueous organic species: implications for germanium and silicon
731 transport and Ge/Si ratio in natural waters. Geochim. Cosmochim. Acta 62, 3413–
732 3428. https://doi.org/10.1016/S0016-7037(98)00249-X
733 Russell, W.A., Papanastassiou, D.A., Tombrello, T.A., 1978. Ca isotope fractionation on the
734 Earth and other solar system materials. Geochim. Cosmochim. Acta 42, 1075–1090.
735 https://doi.org/10.1016/0016-7037(78)90105-9
736 Savage, P.S., Armytage, R.M.G., Georg, R.B., Halliday, A.N., 2014. High temperature
737 silicon isotope geochemistry. Lithos 190–191, 500–519.
738 https://doi.org/10.1016/j.lithos.2014.01.003
739 Schauble, E.A., 2004. Applying Stable Isotope Fractionation Theory to New Systems. Rev.
740 Mineral. Geochem. 55, 65–111. https://doi.org/10.2138/gsrmg.55.1.65
741 Schindelin, J., Arganda-Carreras, I., Frise, E., Kaynig, V., Longair, M., Pietzsch, T.,
742 Preibisch, S., Rueden, C., Saalfeld, S., Schmid, B., Tinevez, J.-Y., White, D.J.,
743 Hartenstein, V., Eliceiri, K., Tomancak, P., Cardona, A., 2012. Fiji: an open-source
744 platform for biological-image analysis. Nat. Methods 9, 676–682.
745 https://doi.org/10.1038/nmeth.2019
746 Schröder, H.C., Wang, X., Tremel, W., Ushijima, H., Müller, W.E.G., 2008. Biofabrication
747 of biosilica-glass by living organisms. Nat. Prod. Rep. 25, 455.
748 https://doi.org/10.1039/b612515h
749 Sillen, L.G., Martell, A.E., 1971. Stability Constants of Metal-Ion Complexes., Suppl.
750 Chemical Society.
751 Sjöberg, S., Ingri, N., Nenner, A.-M., Öhman, L.-O., 1985. Equilibrium and structural
752 studies of silicon(IV) and aluminium(III) in aqueous solution. 12. A potentiometric

753 and 29Si-NMR study of silicon tropolonates. J. Inorg. Biochem. 24, 267–277.
754 https://doi.org/10.1016/0162-0134(85)85055-8
755 Stamm, F.M., Zambardi, T., Chmeleff, J., Schott, J., von Blanckenburg, F., Oelkers, E.H.,
756 2019. The experimental determination of equilibrium Si isotope fractionation factors
757 among H4SiO4o, H3SiO4− and amorphous silica (SiO2·0.32 H2O) at 25 and 75 °C
758 using the three-isotope method. Geochim. Cosmochim. Acta 255, 49–68.
759 https://doi.org/10.1016/j.gca.2019.03.035
760 Tacke, R., Pfrommer, B., Pülm, M., Bertermann, R., 1999. New Chiral Zwitterionic λ5Si-
761 Silicates with an SiO5 or SiO4C Framework: Syntheses, Crystal Structures, and
762 Properties. Eur. J. Inorg. Chem. 1999, 807–816. https://doi.org/10.1002/(SICI)1099-
763 0682(199905)1999:5<807::AID-EJIC807>3.0.CO;2-Y
764 Tesson, B., Lerch, S.J.L., Hildebrand, M., 2017. Characterization of a New Protein Family
765 Associated With the Silica Deposition Vesicle Membrane Enables Genetic
766 Manipulation of Diatom Silica. Sci. Rep. 7, 13457. https://doi.org/10.1038/s41598-
767 017-13613-8
768 Truesdale, V.W., LeCorre, P., 1975. Manuel d'analyse des sels nuritifs dans l'eau de mer:
769 Utilisation de L'autoanalyzer II technicon (r). Université de Bretagne occiendtale,
770 France.
771 Wang, Wei, Jiang, Liu, Lei, Lin, Zhao, 2019. Silicon Isotope Geochemistry: Fractionation
772 Linked to Silicon Complexations and Its Geological Applications. Molecules 24,
773 1415. https://doi.org/10.3390/molecules24071415
774 Wille, M., Sutton, J., Ellwood, M.J., Sambridge, M., Maher, W., Eggins, S., Kelly, M.,
775 2010. Silicon isotopic fractionation in marine sponges: A new model for
776 understanding silicon isotopic variations in sponges. Earth Planet. Sci. Lett. 292,
777 281–289. https://doi.org/10.1016/j.epsl.2010.01.036
778 Zambardi, T., Poitrasson, F., 2011. Precise Determination of Silicon Isotopes in Silicate
779 Rock Reference Materials by MC-ICP-MS. Geostand. Geoanalytical Res. 35, 89–99.
780 https://doi.org/10.1111/j.1751-908X.2010.00067.x
781 Zhang, J., Quay, P.D., Wilbur, D.O., 1995. Carbon isotope fractionation during gas-water
782 exchange and dissolution of CO_2. Geochim. Cosmochim. Acta 59, 107–114.
783 https://doi.org/10.1016/0016-7037(95)91550-D
784 Zhou, Y., Shimizu, K., Cha, J.N., Stucky, G.D., Morse, D.E., 1999. Efficient Catalysis of
785 Polysiloxane Synthesis by Silicateinα Requires Specific Hydroxy and Imidazole
786 Functionalities. Angew. Chem. Int. Ed. 38, 779–782.

https://doi.org/10.1002/(SICI)1521-3773(19990315)38:6<779::AID-ANIE779>3.0.CO;2-#

FIGURE CAPTIONS

Fig. 1. Schematic illustration of the $H_4SiO_4^0$ and the $SiCat_3^{2-}$ aqueous species.

Fig. 2 - Representative images of amorphous SiO_2 powders. A. SEM image of starting powder showing agglomerates of SiO_2 grains. B. TEM image of starting powder showing rounded ~ 21 nm SiO_2 grains. C. Representative SEM image of reacted silica powder. D. TEM image with 40 000x magnification of powder reacted at T ~25°C, pH ~6

Fig. 3. Theoretical equilibrium Si isotopes fractionation factors relative to quartz of Si-diolate (SiDio, open upward pointing triangle), Si- methyllactate (SiLact, open downward pointing triangle), Si-glyconate (SiGly, open circle) and Si-catecholate ($SiCat_3^{2-}$,open diamond), plotted as a function of the mean Si-O distance of the aqueous complex, and comparison with minerals and dissolved species with IV-fold Si coordination (upper left insert). For a more detailed description of the insert, we refer the reader to Fig. 6 of Dupuis et al. (2015). Outside of the insert, black and red symbols correspond to the results of PBE and vdW-DF2 calculations, respectively. The three average points of the Si(IV) minerals (PBE calculations only), and of the Si(V) and Si(VI) compounds (both PBE and vdw-DF2 calculations are considered) are reported (green squares). The regression line going through these three points has the equation $\ln \alpha = -113*(\overline{d}_{Si-O} - 1.626)$.

Fig. 4. Results of ab initio calculations, showing the evolution of the equilibrium fractionation factors between Si-catecholate ($SiCat_3^{2-}$) and silicic acid ($H_4SiO_4^0$; solid line), Si-diolate (SiDiol) and $H_4SiO_4^0$ (dashed line), and $H_3SiO_4^-$ and silicic acid (dotted line) as a function of temperature. Experimental results are shown by square symbols.

Fig. 5 - Plots of pH, Si concentrations and isotopic compositions of solids and aqueous solutions over time during the isotopic exchange experiments. The 2 S.D. uncertainties of data points are denoted by the error bars. Initial values are represented by dashed lines with their 2 S.D. error envelope. A: 0.05 M catechol experiment, B. 0.08 M catechol experiment

Fig. 6. The isotopic composition of the solids (SiO_2,am) and aqueous fluids as a function of the degree of isotope exchange (F) during the isotope exchange experiments. a) 0.05 M catechol experiment (Cat-0.05), and b) 0.08 M catechol experiment (Cat-0.08).

TABLE CAPTIONS

Table 1. Fits of 1000 $\ln\alpha^{30}Si_{Si\ catecholate\text{-}silica}$ and $\alpha^{30}Si_{SiV\text{-}silica}$ based on ax^2+bx^3, with $x=10^3/T(K)$. The resulting fits are is the average of the PBE and the vdW-DF2 calculations, and the uncertainties corresponds to the difference between the two results.

Table 2. Summary of the results of the isotopic exchange experiments performed in this study. Uncertainties of the isotopic measurements are expressed as 2 SD (Standard Deviation) and 2 SE (Standard Error). The 2 SE is computed following the relation: $SE = \frac{SD}{\sqrt{(n-1)}} \times t$, where n denotes the number of measurements performed and t denotes the Student t-factor. δ_{eq} represents the equilibrium isotopic composition of ^{29}Si and *F* denotes the degree of isotopic exchange. [a] denotes the spiked initial solution.

Table 3. Isotopic fractionation factors between catechol bearing fluids and the solid ($\Delta_{eq}{}^{30}Si_{solution\text{-}SiO_2,am}$) together with the average aqueous Si-speciation of the isotope exchange experiments, and the resulting isotopic fractionation factors between $SiCat_3^{2-}$ and SiO_2,am, and the $SiCat_3^{2-}$ and $H_4SiO_4^0$ (H4) aqueous species present in solution. Δ^*_{eq} denotes the equilibrium fractionation factor for the different experiment, whereas Δ_{eq} is the average equilibrium fractionation factor derived from the experiments.

Figures

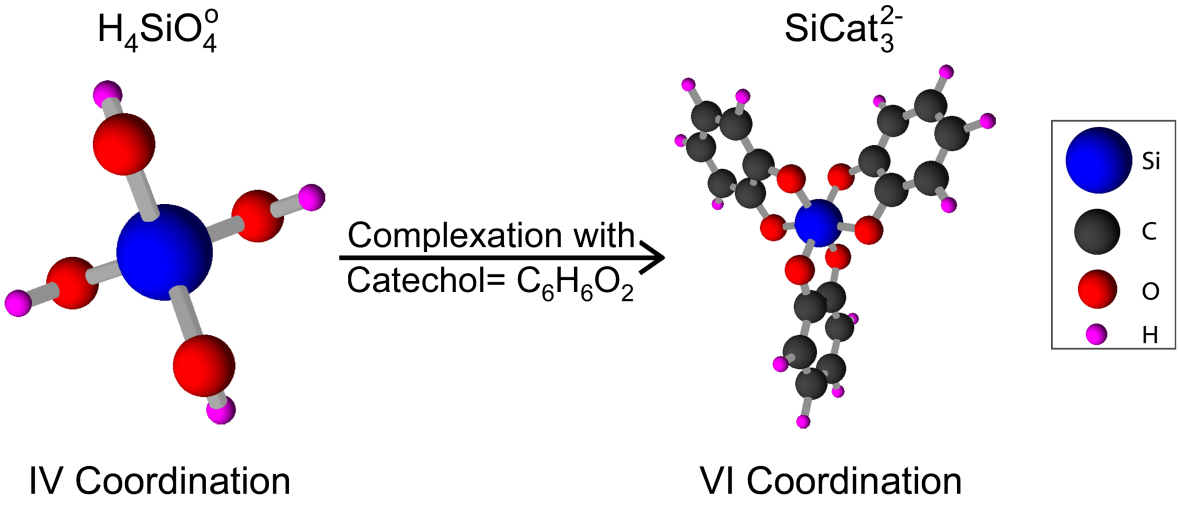

Fig. 1 - Schematic illustration of the $H_4SiO_4°$ and the $SiCat_3^{2-}$ aqueous species.

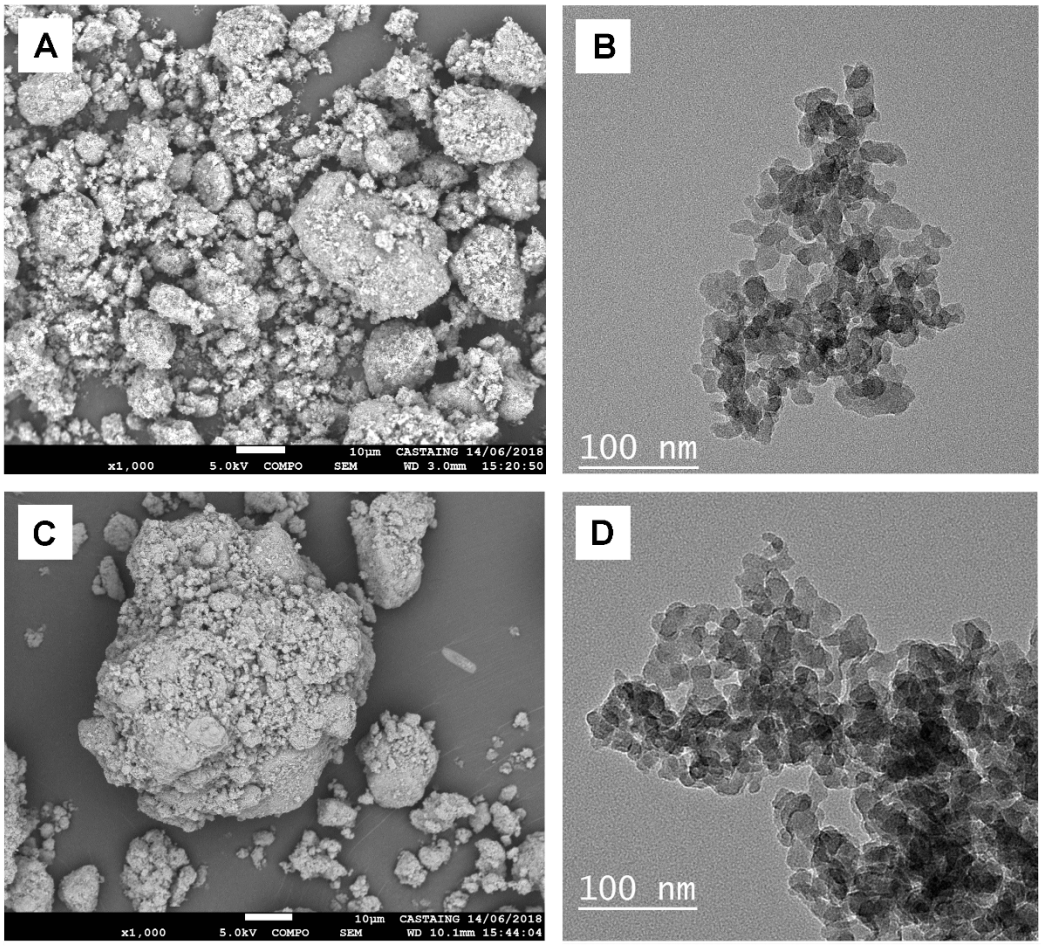

Fig. 2 - Representative images of amorphous SiO_2 powders. A. SEM image of starting powder showing agglomerates of SiO_2 grains. B. TEM image of starting powder showing rounded ~ 21 nm SiO_2 grains. C. Representative SEM image of reacted silicon powder. D. TEM image with 40 000x magnification of powder reacted at T ~25°C, pH ~6

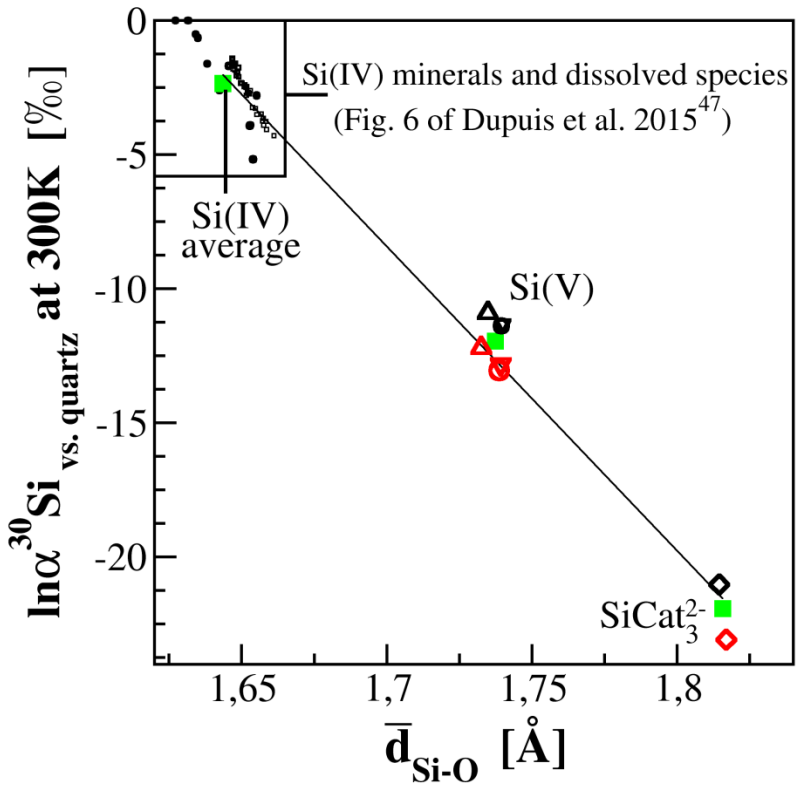

Fig. 3 – Theoretical equilibrium Si isotopes fractionation factors relative to quartz of SiDio (open triangle up), SiLact (open triangle down), SiGly (open circle) and $SiCat_3^{2-}$ (open diamond), plotted as a function of the mean Si-O distance of the aqueous complex, and comparison with minerals and dissolved species with IV-fold Si coordination (upper left insert). For a more detailed description of the insert, we refer the reader to Fig. 6 of Dupuis et al. (2015). Outside of the insert, black and red symbols correspond to the results of PBE and vdW-DF2 calculations, respectively. The three average points of the Si(IV) minerals (PBE calculations only), and of the Si(V) and Si(VI) compounds (both PBE and vdw-DF2 calculations are considered) are reported (green squares). The regression line going through these three points has the equation is $\ln \alpha = -113*(d_0-1.626)$.

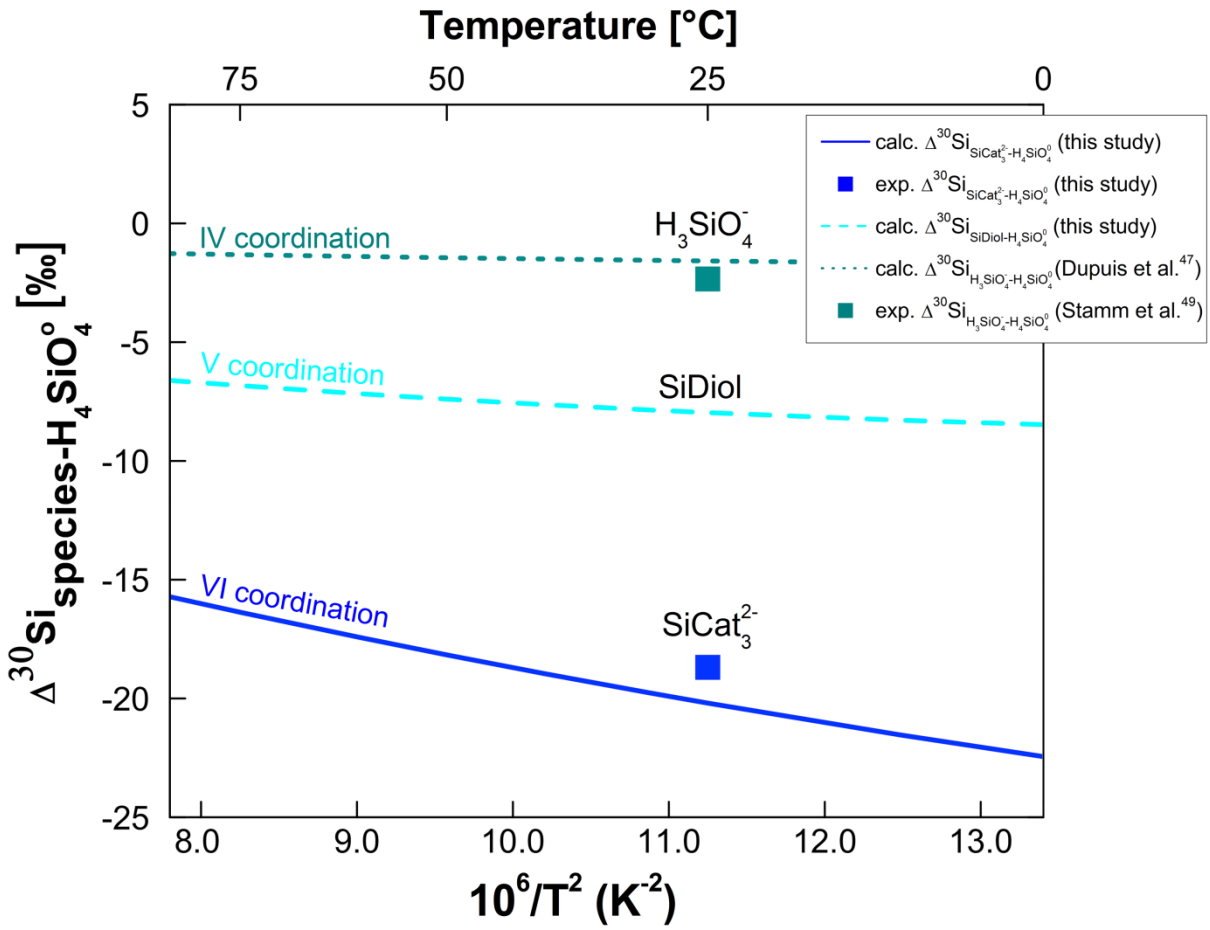

Fig. 4 - Results of ab initio calculations, showing the evolution of the equilibrium fractionation factors between Si-catecholate ($SiCat_3^{2-}$) and silicic acid ($H_4SiO_4^o$; straight line), Si-diolate (SiDiol) and $H_4SiO_4^0$ (dashed line), and $H_3SiO_4^-$ and silicic acid (dotted line) as a function of temperature. Experimental results are shown by square symbols.

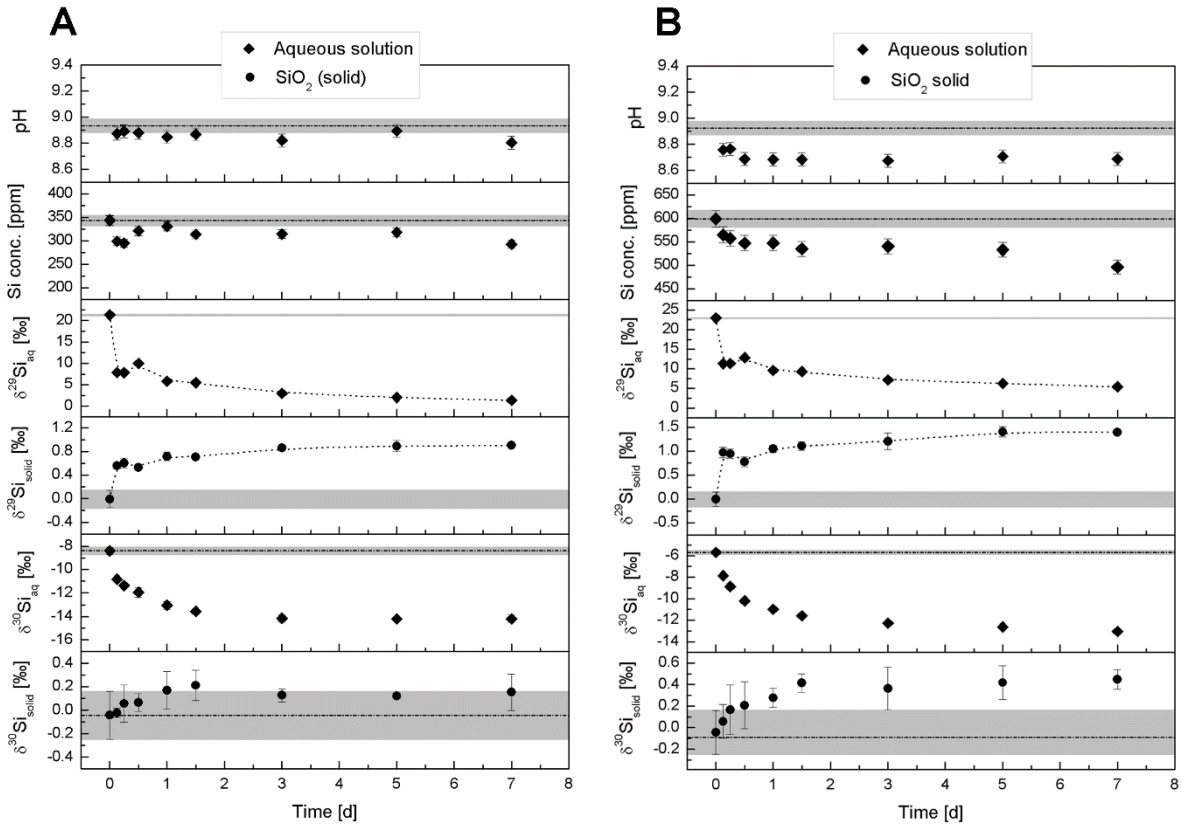

Fig. 5 - Plots of pH, Si concentrations and isotopic compositions of solids and aqueous solutions over time during the isotopic exchange experiments. The 2 S.D. uncertainties of data points are denoted by the error bars. Initial values are represented by dashed lines with their 2 S.D. error envelope. A: 0.05 M catechol experiment, B. 0.08 M catechol experiment

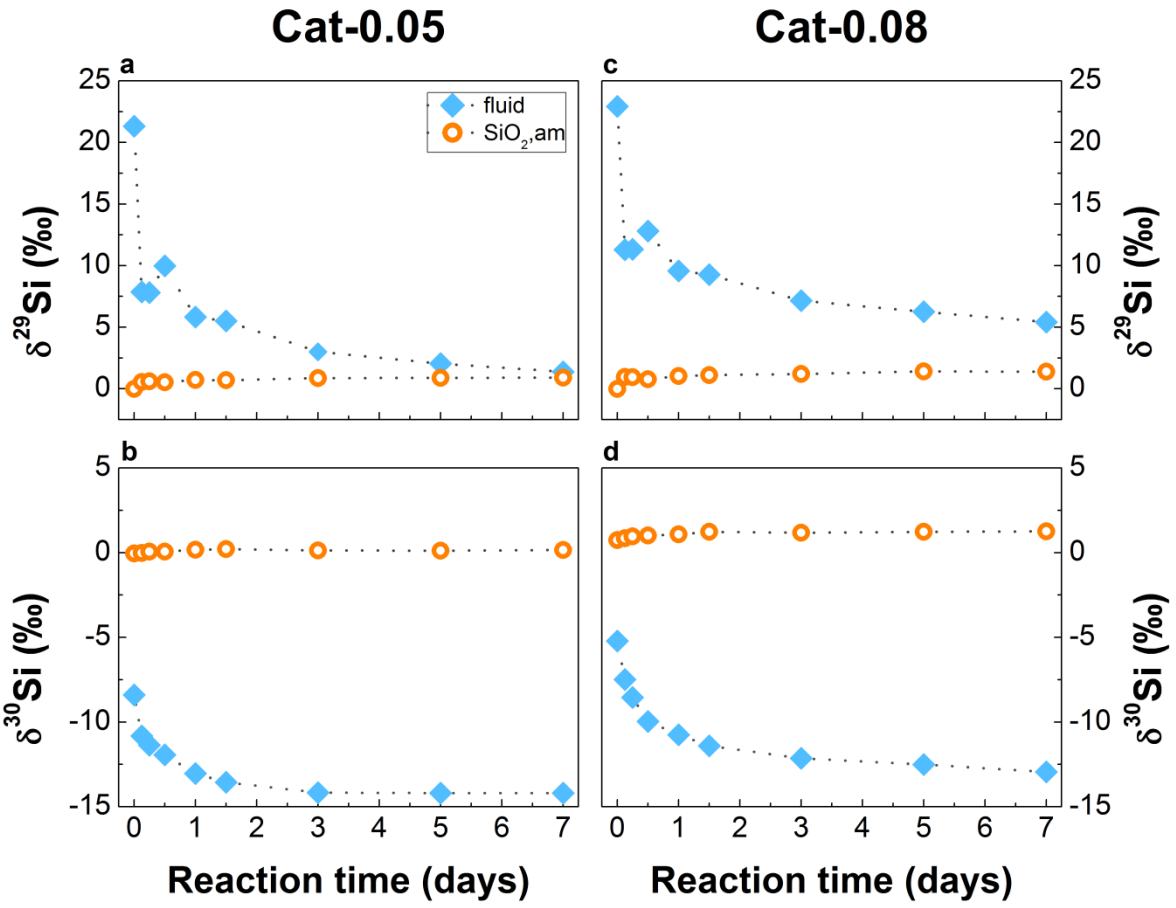

Fig. 6 – Isotopic compositions of solids and aqueous fluids over time during the isotopic exchange experiments of the 0.05 M catechol (Cat-0.05), and 0.08 M catechol (Cat-0.08) experiments. The 2 S.D. uncertainties of data are within the symbol size.

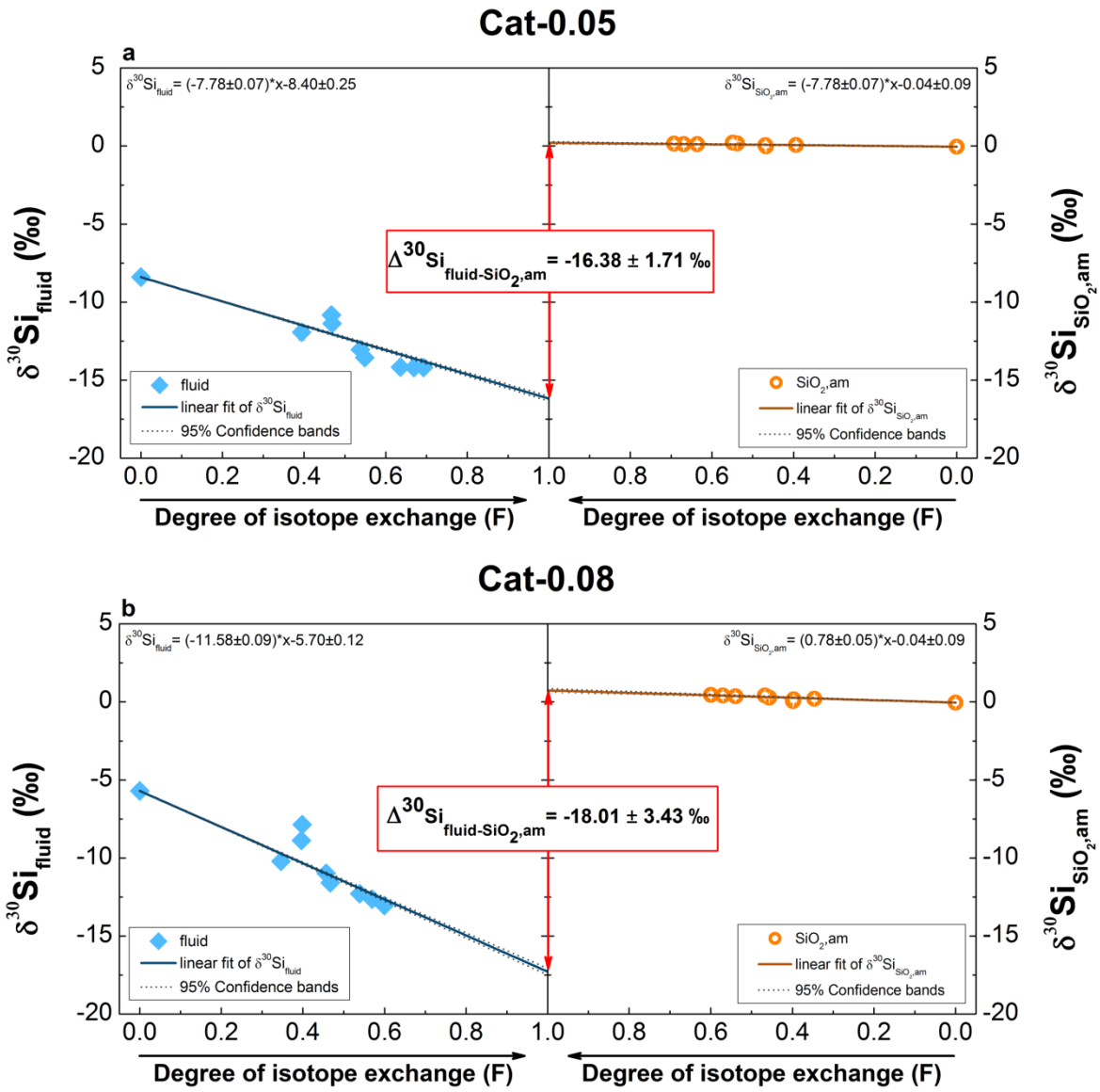

Fig. 7 - The isotopic composition of the solids and aqueous fluids as a function of the degree of isotope exchange (F) during the isotope exchange experiments. a) 0.05 M catechol experiment (Cat-0.05), and b) 0.08 M catechol experiment (Cat-0.08).

Table 1 - Fits of 1000 lnα30SiSi catecholate-silica and α30SiSiV-silica based on ax2 +bx3, with x=103/T(K). The resulting fits are is the average of the PBE and the vdW-DF2 calculations, and the uncertainties corresponds to the difference between the two results.

System	T	Fit parameters		Uncertainties	
	°C	a	b	a	b
SiCat - quartz	0-1100	-3.16	0.354	0.14	-0.011
SiCat - H_4SiO_4	0-50	-3.11	0.392	0.14	-0.011
SiDiol - quartz	0-1100	-1.73	0.205	0.08	-0.008
SiDiol - H_4SiO_4	0-50	-1.54	0.248	0.08	-0.008
SiGly - quartz	0-1100	-1.86	0.226	0.11	-0.010
SiGly - H_4SiO_4	0-50	-1.81	0.268	0.11	-0.010
SiLact - quartz	0-1100	-1.74	0.195	0.08	-0.005
SiLact - H_4SiO_4	0-50	-1.69	0.237	0.08	-0.005

Table 2. Summary of the results of the isotopic exchange experiments performed in this study. Uncertainties of the isotopic measurements are expressed as 2 SD (Standard Deviation) and 2 SE (Standard Error). The 2 SE is computed following the relation: $SE = \frac{SD}{\sqrt{(n-1)}} \times t$, where n denotes the number of measurements performed and t denotes the Student t-factor. δ_{eq} represents the equilibrium isotopic composition of ^{29}Si and F denotes the degree of isotopic exchange. [a] denotes the spiked initial solution.

Exp.	time	pH	Si-conc.	S_{BET}	*solution*						*amorphous SiO_2*						$\delta_{eq}{}^{29}Si$	$F_{sol.}$	ln(1-F)
	[d]		[ppm]	[m^2/g]	$\delta^{30}Si$ [‰]	2SD [‰]	2SE [‰]	$\delta^{29}Si$ [‰]	2SD [‰]	2SE [‰]	$\delta^{30}Si$ [‰]	2SD [‰]	2SE [‰]	$\delta^{29}Si$ [‰]	2SD [‰]	2SE [‰]	[‰]		
0.05 M Catechol																	-7.70		
SigC0.05-0	0	8.9	343	195.6	***-8.60***	*0.27*	*0.22*	***-4.42***	*0.06*	*0.05*	***-0.04***	*0.20*	*0.09*	***-0.01***	*0.15*	*0.07*			
SigC0.05-0 S[a]	0	8.9	345		***-8.40***	*0.32*	*0.26*	***21.31***	*0.14*	*0.11*	***-0.04***	*0.20*	*0.09*	***-0.01***	*0.15*	*0.07*		0.000	0.00
SigC0.05-1	0.125	8.9	300		***-10.83***	*0.12*	*0.10*	***7.87***	*0.02*	*0.02*	***-0.02***	*0.04*	*0.05*	***0.56***	*0.05*	*0.06*		0.463	-0.62
SigC0.05-2	0.25	8.9	295		***-11.37***	*0.08*	*0.07*	***7.81***	*0.03*	*0.02*	***0.06***	*0.16*	*0.10*	***0.60***	*0.08*	*0.05*		0.466	-0.63
SigC0.05-3	0.5	8.9	321		***-11.93***	*0.40*	*0.50*	***9.97***	*0.19*	*0.23*	***0.06***	*0.08*	*0.05*	***0.53***	*0.03*	*0.02*		0.391	-0.50
SigC0.05-4	1	8.8	331		***-13.04***	*0.34*	*0.42*	***5.82***	*0.09*	*0.11*	***0.17***	*0.16*	*0.10*	***0.72***	*0.07*	*0.05*		0.534	-0.76
SigC0.05-5	1.5	8.9	314		***-13.55***	*0.20*	*0.24*	***5.51***	*0.06*	*0.07*	***0.21***	*0.13*	*0.16*	***0.70***	*0.03*	*0.03*		0.545	-0.79
SigC0.05-6	3	8.8	315		***-14.17***	*0.29*	*0.36*	***3.00***	*0.13*	*0.17*	***0.13***	*0.06*	*0.07*	***0.86***	*0.03*	*0.04*		0.631	-1.00
SigC0.05-7	5	8.9	318		***-14.20***	*0.05*	*0.06*	***2.04***	*0.03*	*0.04*	***0.12***	*0.02*	*0.03*	***0.89***	*0.10*	*0.12*		0.664	-1.09
SigC0.05-8	7	8.8	293	174.7	***-14.20***	*0.31*	*0.39*	***1.37***	*0.08*	*0.09*	***0.15***	*0.16*	*0.10*	***0.90***	*0.03*	*0.02*		0.688	-1.16
0.08 M Catechol																	-7.53		
SiC 0.08 0	0	8.9	612	195.6	***-5.73***	*0.24*	*0.19*	***-2.90***	*0.06*	*0.05*	***-0.04***	*0.20*	*0.09*	***-0.01***	*0.15*	*0.07*			
SiC 0.08 0 S[a]	0	8.9	599		***-5.70***	*0.15*	*0.12*	***22.92***	*0.02*	*0.02*	***-0.04***	*0.20*	*0.09*	***-0.01***	*0.15*	*0.07*		0.000	0.00
SiC 0.08 1	0.125	8.8	565		***-7.86***	*0.17*	*0.13*	***11.28***	*0.09*	*0.07*	***0.06***	*0.16*	*0.07*	***0.97***	*0.11*	*0.05*		0.382	-0.48
SiC 0.08 2	0.25	8.8	558		***-8.88***	*0.27*	*0.22*	***11.33***	*0.09*	*0.07*	***0.17***	*0.23*	*0.11*	***0.94***	*0.10*	*0.05*		0.381	-0.48
SiC 0.08 3	0.5	8.7	547		***-10.21***	*0.23*	*0.19*	***12.80***	*0.15*	*0.12*	***0.21***	*0.22*	*0.10*	***0.78***	*0.11*	*0.05*		0.332	-0.40
SiC 0.08 4	1	8.7	547		***-10.97***	*0.14*	*0.11*	***9.57***	*0.06*	*0.05*	***0.28***	*0.09*	*0.04*	***1.04***	*0.07*	*0.03*		0.438	-0.58
SiC 0.08 5	1.5	8.7	535		***-11.59***	*0.16*	*0.13*	***9.27***	*0.04*	*0.03*	***0.41***	*0.08*	*0.04*	***1.11***	*0.09*	*0.04*		0.448	-0.59
SiC 0.08 6	3	8.7	540		***-12.28***	*0.09*	*0.07*	***7.16***	*0.07*	*0.06*	***0.36***	*0.20*	*0.09*	***1.21***	*0.17*	*0.08*		0.518	-0.73
SiC 0.08 7	5	8.7	533		***-12.63***	*0.14*	*0.11*	***6.26***	*0.06*	*0.04*	***0.42***	*0.16*	*0.07*	***1.40***	*0.11*	*0.05*		0.547	-0.79
SiC 0.08 8	7	8.7	496	165.6	***-13.04***	*0.03*	*0.02*	***5.41***	*0.08*	*0.06*	***0.45***	*0.09*	*0.05*	***1.39***	*0.06*	*0.03*		0.575	-0.86

Table 3. Isotopic fractionation factors between catechol bearing fluids and the solid ($\Delta_{eq}{}^{30}Si_{solution\text{-}SiO_2,am}$) together with the average aqueous Si-speciation of the isotope exchange experiments, and the resulting isotopic fractionation factors between $SiCat_3^{2-}$ and SiO_2,am, and the $SiCat_3^{2-}$ and $H_4SiO_4^0$ (H4) aqueous species present in solution. Δ^*_{eq} denotes the equilibrium fractionation factor for the different experiment, whereas Δ_{eq} is the average equilibrium fractionation factor derived from the experiments.

					Speciation			Equilibrium fractionation factors							
Exp.	pH	Si conc. (mmol)	$\Delta_{eq}{}^{30}Si_{solution\text{-}SiO_2,am}$ (‰)	err (‰)	Si-Cat (%)	$H_4SiO_4^0$ (%)	$H_3SiO_4^-$ (%)	$\Delta_{eq}{}^{30}Si_{SiCat_3^{2-}\text{-}SiO_2,am}$ (‰)	err (‰)	$\Delta^*_{eq}{}^{30}Si_{SiCat_3^{2-}\text{-}H4}$ (‰)	err (‰)	**$\Delta_{eq}{}^{30}Si_{SiCat_3^{2-}\text{-}H4}$ (‰)**	**err (‰)**	$\Delta_{eq}{}^{30}Si_{H3\text{-}H4}$ (‰)	err (‰)
Cat-0.05	8.87	4.05	-16.45	1.71	87.26	12.74		-18.71	0.86	-18.26	0.44	**-18.69**	**0.49**		
Cat-0.08	8.74	8.48	-18.60	3.43	91.83	8.17		-19.57	1.72	-19.12	0.86				
SibA[a]	6.37	1.79	-0.45	0.20		100.00									
SibB[a]	9.84	4.05	-1.63	0.23		49.63	50.37							-2.34	0.13

[a] data from Stamm et al. (2019)

Supplemental Information

Supplemental Information A - Validation of ab initio calculations

Supplemental Table A.1 – Lattice parameters determined after relaxation of the compounds considered in this study, and comparison with experiment

Si(VI) Cat	PBE [Δ_{exp} (%)]	VdW-DF2 [Δ_{exp} (%)]	Exp[a]
a (Å)	12.0599 [+2.5]	11.7441 [-0.2]	11.7680(13)
b (Å)	12.7784 [+3.1]	12.3805 [-0.1]	12.3986(13)
c (Å)	14.2177 [+3.0]	13.7437 [-0.4]	13.7981(15)
α (°)	79.940	80.069	79.833(9)
β (°)	80.821	81.370	81.158(10)
γ (°)	63.759	63.424	63.676(10)
<d(Si-O)> (Å)	1.8145 [+1.8]	1.8169 [+1.9]	1.783
Si(V) Dio	PBE [Δ_{exp} (%)]	VdW-DF2 [Δ_{exp} (%)]	Exp[b]
a (Å)	5.8524 [+5.5]	5.6345 [+1.6]	5.5453(10)
b (Å)	19.252 [+3.3]	18.832 [+1.1]	18.635(3)
c (Å)	11.0464 [+1.8]	10.9782 [+1.2]	10.8478(19)
β (°)	90.17	90.06	90.07(2)
<d(Si-O)> (Å)	1.7348 [+2.5]	1.7325 [+2.4]	1.692(1)
Si(V) Lact	PBE [Δ_{exp} (%)]	VdW-DF2 [Δ_{exp} (%)]	Exp[c]
a (Å)	6.902 [+4.4]	6.606 [-0.07]	6.611(2)
b (Å)	19.155 [+2.8]	18.640 [+0.04]	18.633(4)
c (Å)	14.587 [+1.8]	14.336 [+0.06]	14.328(4)
β (°)	102.56	102.97	103.04(3)
<d(Si-O)> (Å)	1.7399 [+2.0]	1.7392 [+2.0]	1.705(1)
Si(V) Gly	PBE [Δ_{exp} (%)]	VdW-DF2 [Δ_{exp} (%)]	Exp[d]
a (Å)	8.081 [+1.2]	7.996 [+0.09]	7.989(2)
b (Å)	8.882 [+1.3]	8.837 [+0.8]	8.770(2)
c (Å)	13.867 [+3.8]	13.278 [-0.6]	13.362(2)
<d(Si-O)> (Å)	1.7394 [+1.5]	1.7388 [+1.4]	1.714(1)
Si(IV) Quartz	PBE [Δ_{exp} (%)]	VdW-DF2 [Δ_{exp} (%)]	Exp[e]
a (Å)	5.019543 [+2.2]	4.991477 [+1.6]	4.913437
c (Å)	5.509680 [+1.9]	5.492876 [+1.6]	5.405118
<d(Si-O)> (Å)	1.62816 [+1.3]	1.62505 [+1.1]	1.60803

[a] Hahn *et al.* (1995) , $Li_2[Si(cat)_3]$•3.5dme structure **;** [b] Benner *et al*. (1999) ; [c] Tacke *et al*. (1999) , compound **7** ; [d] Donhärl *et al*. (1998) , compound **1 ;** [e] Antao et al., 2008

In this study, we assessed the fractionation of Si isotopes at equilibrium between various compounds which, except for quartz, are molecular crystals where weak dispersion forces play an important role, quite differently from previous calculations on silicate minerals (Méheut et al., 2007; Méheut et al., 2009; Méheut and Schauble, 2014; Huang et al., 2014). Previous calculations were based on the PBE functional (Perdew et al. 1996), which by construction miss dispersion effects. Improved functionals, meant to better account for dispersion (yet at higher numerical costs) have been designed. Here, we used the vdW-DF2 non-local functional (Lee et al. 2010), as an improvement over the PBE functional in this system.

Table A.1 shows the structural parameters of the relaxed structures of quartz, and of 4 molecular crystals containing Si hypervalent organic complexes. As expected, the two functionals give similar results for quartz, with cell parameters over-estimated by 1-2% compared to experiment. Also as expected, they give different results for the molecular crystals, PBE overestimating quite significantly the cell parameters (by 3-4% typically) whereas vdW-DF2 gives much closer agreement with experiment. Note, however, that in all cases, the Si-O distances given by the two functionals are very similar, and overestimate experiment by ~2%, as typical for calculations of silicate minerals based on PBE (Méheut and Schauble, 2014).

Looking at Si equilibrium fractionation properties (Figure 2), the calculated fractionation between those molecular crystals and quartz are systematically more negative when the vdW-DF2 functional is employed, by 11 to 15%.

To look at this effect into more detail, we represented in Figure A.1 the β-factors of some of the studied compounds. Somewhat consistently with the effect described on cell parameters (see Table 1), it shows that the choice of functional has a negligible effect on the calculated fractionation properties for quartz, whereas for the Si(V) species, vdW-DF2 gives β-factors smaller by ~2% (-1.10‰ at 300K) compared to PBE. For the Si(VI) species, this difference reaches 5% (-2.12‰ at 300K).

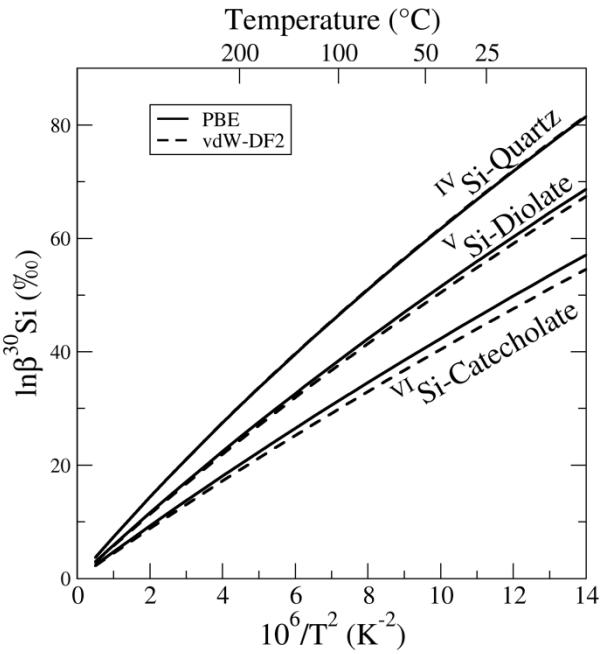

Supplemental Figure A.1 – Calculated logarithmic β-factors for compounds representative of IV-fold, V-fold and VI-fold Si.

Because fractionation properties directly depend on vibrational properties, we compare in Figure A.2 the calculated vibrational frequencies of quartz with their experimental equivalent. For both functionals, the calculated frequencies underestimate experimental values by ~ 5% (see insert of Figure A.2), as typical for the PBE functional (Méheut and Schauble, 2014) . Looking into more details, vdW-DF2 gives higher frequencies than PBE for modes below ~600 cm^{-1}, but for the modes that are important for Si isotopes fractionation, at high frequencies, both functionals give indistinguishable results. To illustrate this last statement, we estimated the contribution of each vibrational frequency at gamma to the overall β-factor. The result for quartz is shown on Figure A.3. We can see once again that vdW-DF2 frequencies (dashed sticks) tend to be larger than those generated from PBE for low frequency modes, whereas they are slightly below for high frequency modes. Around 750 cm^{-1}, both functionals give the same result. In terms of fractionation, the important modes (between 750 and 1250 cm^{-1}) have very similar frequencies and contribution.

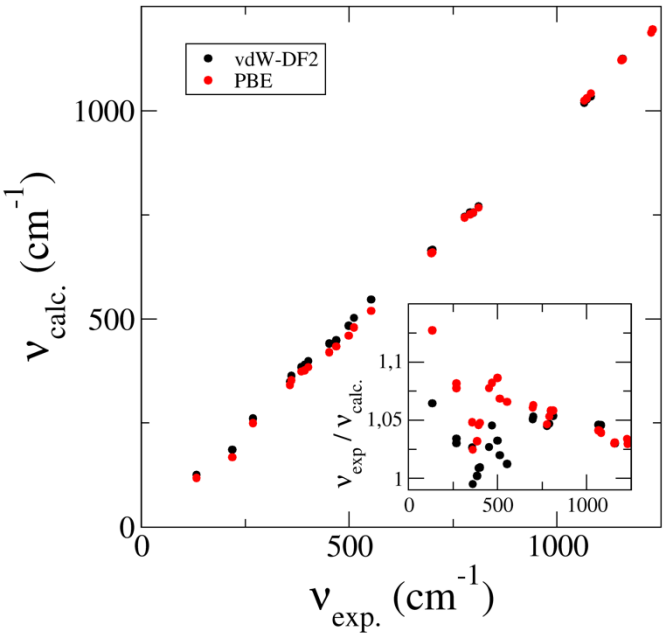

Supplemental Figure A.2 – Comparison of experimental and calculated vibrational frequencies, for the two density functionals tested in this study. Insert: ratio between experimental and theoretical frequencies.

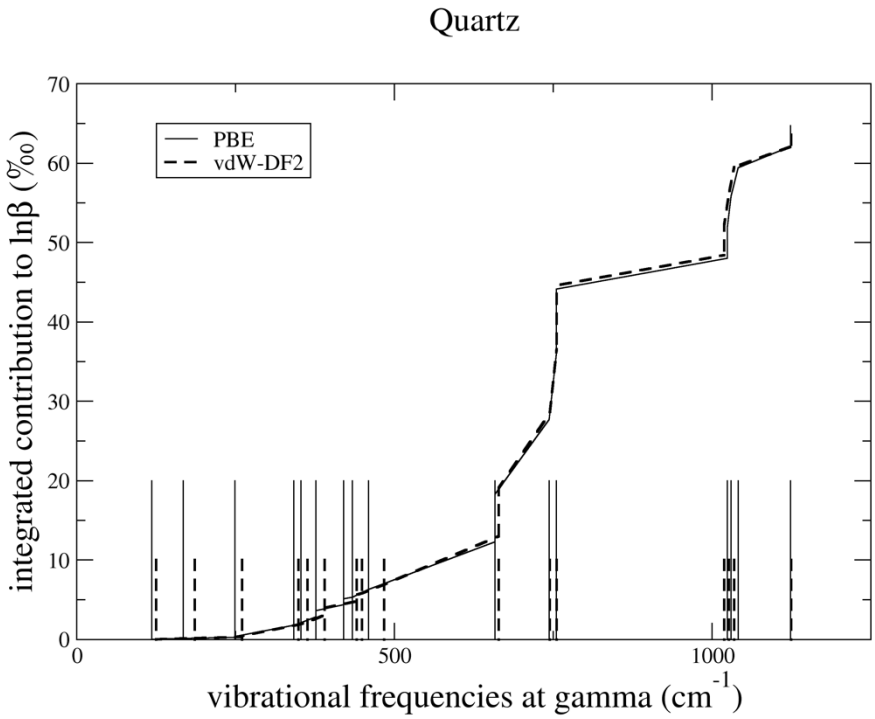

Supplemental Figure A.3 – Vibrational analysis of the Si β-factor of quartz. Sticks represent the positions of the TO modes of quartz at the Γ-point, and the contribution of each of these frequencies is integrated to give the monotonous curve. Solid line: PBE calculations; dashed line: vdW-DF2 calculation.

For the V-fold and VI-fold coordinated compounds considered in this study, we performed the same vibrational analysis as for quartz. Figure A.4 shows a typical example for the V-fold coordinated Si-diolate. Since these compounds contain more atoms per unit cell than quartz, their vibrational frequencies are more numerous, and their vibrational analysis is more difficult to interpret. For this reason, on Figure A.4 we focused on the most important contributions. We can see however that frequencies representing major contributions can be identified, for example around 685 and 775 cm^{-1}, and that these contributions systematically occur at lower frequencies for the vdW-DF2 calculation, leading to a smaller contribution, and ultimately to a smaller β-factor. It is however difficult to determine if this leads to a better accuracy of vdW-DF2 without experimental data for the vibrational frequencies of these molecular compounds

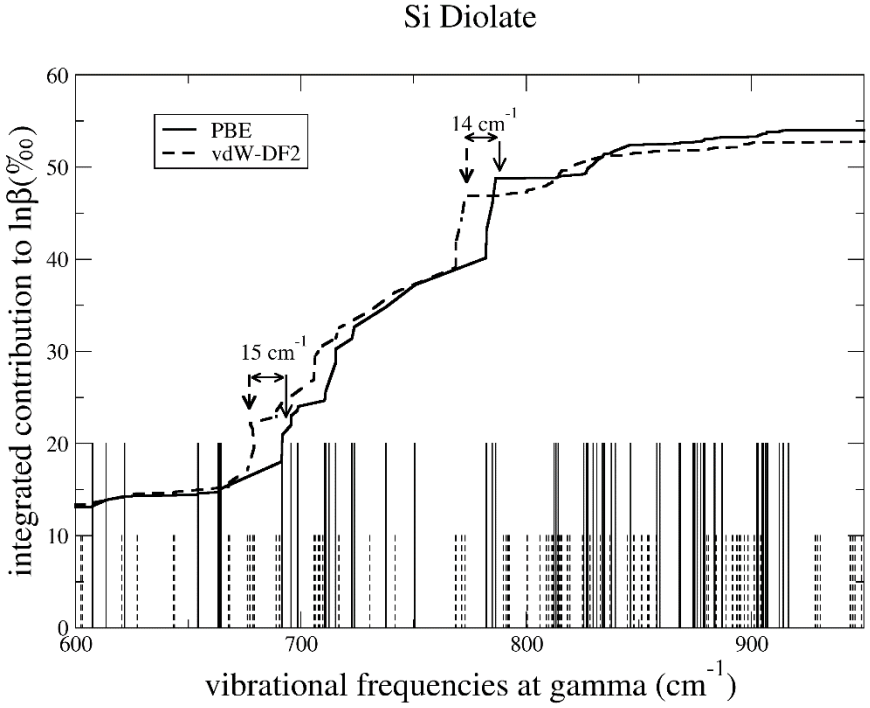

Supplemental Figure A.4 – Vibrational analysis of the Si β-factor of SiDio. The horizontal scale has been limited to focus on the main contributions. See legend of Figure A.3 for details.

Independently of Si-O distances, vdW-DF2 therefore leads to significantly lower vibrational frequencies and lower β-factors for the molecular crystals considered here, whereas it gives results very similar to PBE for quartz. Without experimental data for the vibrational frequencies of those molecular compounds, it is not possible to definitely determine which functional is the more accurate. Instead, we chose to consider the difference between the two calculations as an estimate of the uncertainty of those calculations.

Supplemental Information B

The supplemental information B provides additional data, describing the experimental results of this study.

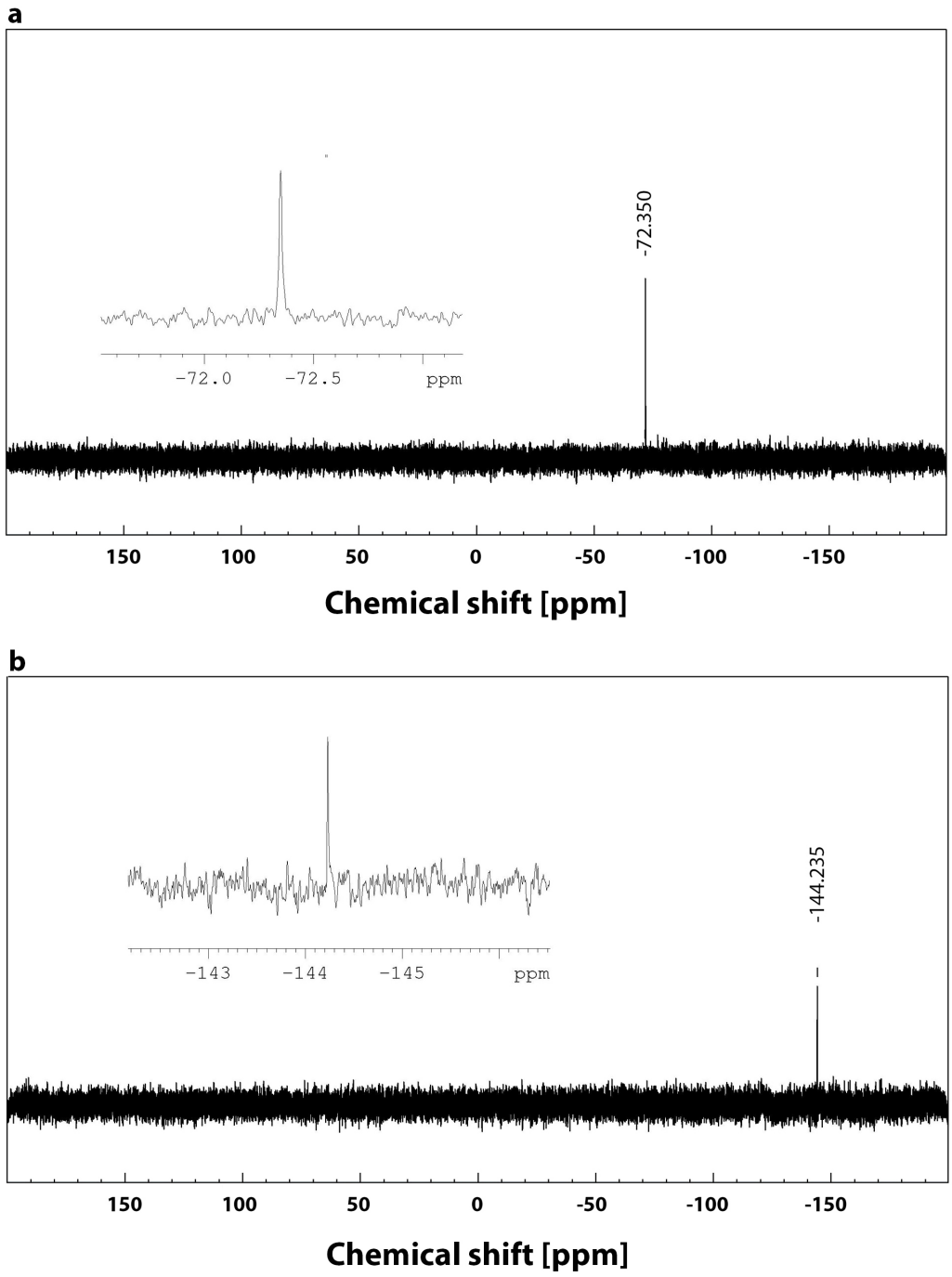

Supplemental Figure B.1 – ^{29}Si NMR spectra of a) a 1.8 mM catechol-free silica solution of pH = 10.1, and b) a 1.8 mM silica solution of pH = 8.9 containing 0.05 M catechol.

Supplemental Table B.1 - Summary of dissociation constants added to the PHREEQC llnl database and their source.

Reaction	log K	Source
$SiO_2 + 2\ H_2O \leftrightarrow H_4SiO_4^o$	-2.80	Stamm et al.[49]
$H_2Cat^o \leftrightarrow HCat^- + H^+$	-9.45	Sillen & Martell[78]
$H_2Cat^o \leftrightarrow HCat^{2-} + 2\ H^+$	-22.45	Sillen & Martell[78]
$SiO_2 + 3\ H_2Cat \leftrightarrow SiCat_3^{--} + 2\ H^+ + 2\ H_2O$	-12.00	Pokrovski & Schott[31]

Supplemental Table B.2 - Overview of the chemical equilibration of amorphous silica with the 0.05 (SigC0.05) and 0.08 (SigC0.08) mol/kg aqueous catechol solution at 25 °C during the first step of the two experimental series.

Exp.	T [°C]	Time [d]	pH	Si-conc. [ppm]	Si-conc. [mmol/kg]
SigC0.05:					
	25	0	9.0	0	0.00
	25	1	9.2	158	5.63
	25	4	8.9	300	10.67
	25	9	9.0	354	12.61
	25	10	9.0	343	12.22
SigC0.08:					
	25	0	9.1	0	0.00
	25	1	9.0	219	7.81
	25	4	9.0	332	11.80
	25	7	9.0	537	19.13
	25	10	8.9	611	21.75

Supplemental Table B.3 – Calculation of the possible bias introduced to the measurements by a 3 % contamination with a natural abundance

Sample	δ^{30} Si sol.	2 SD	Contamination						δ^{29} Si sol.	2 SD	Contamination						δ^{30} SiO_2	2 SD	Contamination			
ID	[‰]	[‰]	-1 ‰	Δmeas-cont.	0 ‰	Δmeas-cont.	1 ‰	Δmeas-cont.	[‰]	[‰]	-1 ‰	Δmeas-cont.	0 ‰	Δmeas-cont.	1 ‰	Δmeas-cont.	[‰]	[‰]	-1 ‰	Δmeas-cont.	0 ‰	Δmeas
SigC-0.05-0	***-8.60***	***0.27***	*-8.84*	*0.24*	*-8.87*	*0.27*	*-8.90*	*0.30*	***-4.42***	***0.06***	*-4.53*	*0.11*	*-4.56*	*0.14*	*-4.59*	*0.17*	***-0.04***	***0.20***	*-0.01*	*0.03*	*-0.05*	*0.0*
SigC-0.05-0 S	***-8.40***	***0.32***	*-8.63*	*0.23*	*-8.66*	*0.26*	*-8.69*	*0.29*	***21.31***	***0.14***	*22.00*	*0.69*	*21.97*	*0.66*	*21.94*	*0.63*	***-0.04***	***0.20***	*-0.01*	*0.03*	*-0.05*	*0.0*
SigC-0.05-1	***-10.83***	***0.12***	*-11.13*	*0.30*	*-11.16*	*0.33*	*-11.19*	*0.37*	***7.87***	***0.02***	*8.14*	*0.27*	*8.11*	*0.24*	*8.08*	*0.21*	***-0.02***	***0.04***	*0.01*	*0.03*	*-0.02*	*0.0*
SigC-0.05-2	***-11.37***	***0.08***	*-11.69*	*0.32*	*-11.72*	*0.35*	*-11.75*	*0.38*	***7.81***	***0.03***	*8.08*	*0.27*	*8.05*	*0.24*	*8.02*	*0.21*	***0.06***	***0.16***	*0.09*	*0.03*	*0.06*	*0.0*
SigC-0.05-3	***-11.93***	***0.40***	*-12.27*	*0.34*	*-12.30*	*0.37*	*-12.33*	*0.40*	***9.97***	***0.19***	*10.31*	*0.34*	*10.28*	*0.31*	*10.25*	*0.28*	***0.06***	***0.08***	*0.10*	*0.03*	*0.07*	*0.0*
SigC-0.05-4	***-13.04***	***0.34***	*-13.42*	*0.37*	*-13.45*	*0.40*	*-13.48*	*0.43*	***5.82***	***0.09***	*6.03*	*0.21*	*6.00*	*0.18*	*5.97*	*0.15*	***0.17***	***0.16***	*0.20*	*0.04*	*0.17*	*0.0*
SigC-0.05-5	***-13.55***	***0.20***	*-13.94*	*0.39*	*-13.97*	*0.42*	*-14.00*	*0.45*	***5.51***	***0.06***	*5.71*	*0.20*	*5.68*	*0.17*	*5.65*	*0.14*	***0.21***	***0.13***	*0.25*	*0.04*	*0.22*	*0.0*
SigC-0.05-6	***-14.17***	***0.29***	*-14.57*	*0.41*	*-14.61*	*0.44*	*-14.64*	*0.47*	***3.00***	***0.13***	*3.12*	*0.12*	*3.09*	*0.09*	*3.06*	*0.06*	***0.13***	***0.06***	*0.16*	*0.03*	*0.13*	*0.0*
SigC-0.05-7	***-14.20***	***0.05***	*-14.61*	*0.41*	*-14.64*	*0.44*	*-14.67*	*0.47*	***2.04***	***0.03***	*2.14*	*0.09*	*2.11*	*0.06*	*2.08*	*0.03*	***0.12***	***0.02***	*0.16*	*0.03*	*0.13*	*0.0*
SigC-0.05-8	***-14.20***	***0.31***	*-14.61*	*0.41*	*-14.64*	*0.44*	*-14.67*	*0.47*	***1.37***	***0.08***	*1.44*	*0.07*	*1.41*	*0.04*	*1.38*	*0.01*	***0.15***	***0.16***	*0.19*	*0.04*	*0.16*	*0.0*
SigC-0.08-0	***-5.73***	***0.24***	*-5.87*	*0.15*	*-5.90*	*0.18*	*-5.93*	*0.21*	***-2.90***	***0.06***	*-2.96*	*0.06*	*-2.99*	*0.09*	*-3.02*	*0.12*	***-0.04***	***0.20***	*-0.01*	*0.03*	*-0.05*	*0.0*
SigC-0.08-0 S	***-5.70***	***0.15***	*-5.85*	*0.15*	*-5.88*	*0.18*	*-5.91*	*0.21*	***22.92***	***0.02***	*23.66*	*0.74*	*23.63*	*0.71*	*23.60*	*0.68*	***-0.04***	***0.20***	*-0.01*	*0.03*	*-0.05*	*0.0*
SigC-0.08-1	***-7.86***	***0.17***	*-8.08*	*0.21*	*-8.11*	*0.24*	*-8.14*	*0.27*	***11.28***	***0.09***	*11.66*	*0.38*	*11.63*	*0.35*	*11.60*	*0.32*	***0.06***	***0.16***	*0.09*	*0.03*	*0.06*	*0.0*
SigC-0.08-2	***-8.88***	***0.27***	*-9.12*	*0.24*	*-9.15*	*0.27*	*-9.18*	*0.31*	***11.33***	***0.09***	*11.71*	*0.38*	*11.68*	*0.35*	*11.65*	*0.32*	***0.17***	***0.23***	*0.20*	*0.04*	*0.17*	*0.0*
SigC-0.08-3	***-10.21***	***0.23***	*-10.50*	*0.28*	*-10.53*	*0.32*	*-10.56*	*0.35*	***12.80***	***0.15***	*13.23*	*0.43*	*13.20*	*0.40*	*13.17*	*0.36*	***0.21***	***0.22***	*0.24*	*0.04*	*0.21*	*0.0*
SigC-0.08-4	***-10.97***	***0.14***	*-11.28*	*0.31*	*-11.31*	*0.34*	*-11.34*	*0.37*	***9.57***	***0.06***	*9.90*	*0.33*	*9.87*	*0.30*	*9.84*	*0.27*	***0.28***	***0.09***	*0.32*	*0.04*	*0.28*	*0.0*
SigC-0.08-5	***-11.59***	***0.16***	*-11.92*	*0.33*	*-11.95*	*0.36*	*-11.98*	*0.39*	***9.27***	***0.04***	*9.59*	*0.32*	*9.56*	*0.29*	*9.53*	*0.26*	***0.41***	***0.08***	*0.46*	*0.04*	*0.43*	*0.0*
SigC-0.08-6	***-12.28***	***0.09***	*-12.63*	*0.35*	*-12.66*	*0.38*	*-12.69*	*0.41*	***7.16***	***0.07***	*7.41*	*0.25*	*7.38*	*0.22*	*7.35*	*0.19*	***0.36***	***0.20***	*0.40*	*0.04*	*0.37*	*0.0*
SigC-0.08-7	***-12.63***	***0.14***	*-12.99*	*0.36*	*-13.02*	*0.39*	*-13.06*	*0.42*	***6.26***	***0.06***	*6.48*	*0.22*	*6.45*	*0.19*	*6.42*	*0.16*	***0.42***	***0.16***	*0.46*	*0.04*	*0.43*	*0.0*
SigC-0.08-8	***-13.04***	***0.03***	*-13.41*	*0.37*	*-13.45*	*0.40*	*-13.48*	*0.43*	***5.41***	***0.08***	*5.61*	*0.20*	*5.57*	*0.17*	*5.54*	*0.14*	***0.45***	***0.09***	*0.49*	*0.04*	*0.46*	*0.0*

Additional References

[a]Antao, S.M., Hassan, I., Wang, J., Lee, P.L., Toby, B.H., 2008. STATE-OF-TH HIGH-RESOLUTION POWDER X-RAY DIFFRACTION (HF ILLUSTRATED WITH RIETVELD STRUCTURE REFINEMENT OF QU SODALITE, TREMOLITE, AND MEIONITE. Can. Mineral. 46, 150 https://doi.org/10.3749/canmin.46.5.1501